THESIS

FABRICATION AND CHARACTERIZATION OF EPOXY RESIN AND CARBON/EPOXY COMPOSITE LAMINATES CONTAINING CARBON NANOFIBERS AND NANOTUBES

Thesis

Submitted to

School of Engineering

UNIVERSITY OF DAYTON

In Partial Fulfillment of the Requirements for

The Degree

Master of Science in Chemical Engineering

By

Regina Estee Donaldson

UNIVERSITY OF DAYTON

Dayton, Ohio

August, 2007

FABRICATION AND CHARACTERIZATION OF EPOXY RESIN AND CARBON/EPOXY COMPOSITE LAMINATES CONTAINING CARBON NANOFIBERS AND NANOTUBES

APPROVED BY:

ABSTRACT

FABRICATION AND CHARACTERIZATION OF EPOXY RESIN AND CARBON/EPOXY COMPOSITE LAMINATES CONTAINING CARBON NANOFIBERS AND NANOTUBES

Name: Donaldson, Regina Estee
University of Dayton

Research Advisor: Dr. Donald Klosterman

Vapor grown carbon nanofibers (VGCF) and Single and Multi-walled carbon nanotubes (CNTs) were dispersed into a model epoxy/amine resin at a level of 8 wt% and 0.15 wt% respectively, using a high shear, solvent-free process. Four batches of VGCF which differed in the amount of surface oxidation were used in this study, in addition to two control batches of non-oxidized VGCF. One batch each of non-oxidized and oxidized CNTs were used to prepare several epoxy samples with varying viscosity. The resulting resin mixtures were evaluated for dispersion quality, and then cured under heat and pressure to form solid plaques. Samples were then evaluated for glass transition temperature (T_g), flexure strength, and Izod impact strength. The Izod impact fracture surfaces were examined with Scanning Electron Microscopy (SEM). The dispersion quality varied from batch to batch, with batches containing oxidized VGCFs generally containing fewer and smaller

agglomerated nanofibers than those containing non-oxidized VGCFs. The T_g values of the nanofiber-epoxy composites were the same or up to 7°C higher than a neat resin sample. Flexure modulus and strength varied from batch to batch, but one batch showed a 237% increase in modulus and 29% increase in flexure strength over neat resin. This same batch also exhibited a 24% increase in Izod impact strength compared to neat resin, although other batches performed more poorly than neat resin. The CNT samples resulted in higher (up to 11%) impact strength than the neat resin, but data scatter was too high (40%) to make the differences statistically significant. Additional nanofiber/resin mixtures were prepared and used to demonstrate the production of carbon fiber composite laminates using a resin film interleaving technique. The impact strength of the carbon fiber laminates containing VGCFs was about 73% higher than those containing no VGCF, and the data scatter was lower (~10%). This result demonstrates that out-of-plane mechanical properties of composite laminates can be improved by incorporating a nano-modified matrix.

ACKNOWLEDGMENTS

I would like to thank my research advisor, Dr. Donald Klosterman, for allowing me to work with him in polymer/nanocomposite research. His polymer science course as well as the hands-on experience gained during this study ignited an interest in materials engineering that I may have not considered.

Thanks to Dr. Charles Browning and Mr. Maceo Coefield for accepting me to participate in the Clarkson and Minority Leaders Programs. Without this opportunity to work as a graduate research assistant, I would have had a difficult time locating valuable resources to research and complete my thesis requirement.

Special thanks to Dr. Tony Saliba and the Chemical Engineering department for allowing me to pursue a chemical engineering degree at the University of Dayton, especially given that I have a mechanical engineering background. I am gracious for all of the encouragement and kindness shown, which will always be remembered.

This research and my education were supported primarily by the Clarkson program. Also, partial support was provided by Systran Federal Corporation (SFC) in collaboration with the Phase I STTR (project FN Composites-1 contract #N00014-06-M-0320 STTR program funding, Office of Naval Research). The Dayton Area Graduate Studies Institute (DAGSI) is gratefully acknowledged for awarding me a tuition scholarship.

The author wishes to thank Melissa Williams for T_g and flexure testing data; Makeeba Anderson and Kevin Washington for assisting with dispersion of nanomaterials and fabricating samples; Khalid Lafdi (UDRI) for supplying oxidized carbon nanofibers; Tom Wittberg (UDRI) for XPS results; Dale Grant (UDRI) for composite laminate photomicrographs and use of cutting saw and microscope equipment; UDRI nanocomposites group for use of dispersion, hot press, wet saw, and film forming equipment; UDRI Elastomers & Composites Group (Roger Rondeau, Jarod Stonecash) for use of Izod impact unit; UDRI Advanced Polymers Group for use of TMA equipment; UD Mechanical Engineering Department for use of Instron; and the UD Nanoscale Engineering Science and Technology (NEST) Center for use of the HRSEM unit.

TABLE OF CONTENTS

LIST OF FIGURES

LIST OF TABLES

CHAPTER I

INTRODUCTION

Several researchers have performed extensive investigations of carbon nanotubes (CNTs) since their discovery by Sumio Iijima in 1991 [1]. Their inherently high mechanical, electrical and thermal properties have made them ideal candidates to improve the properties of other materials with which they can be mixed [2, 3]. Their low density, fiber-like structure, and high aspect ratio (length/diameter) have fueled development of nanotube-reinforced composite materials, where the extraordinary stiffness, strength, and elasticity of the nanotube may lead to a new class of engineering materials [4]. Previous researchers have reported that CNTs possess a tensile modulus and strength as high as 1 TPa and 200 GPa, respectively [5]. Applications that could use these materials include devices in nanoelectronics, field emitters, and structural components. The types of CNTs used in these applications are Single-walled Carbon Nanotubes (SWNTs), Double-walled Carbon Nanotubes (DWNTs) or Multi-walled Carbon Nanotubes (MWNTs). The availability and cost of CNTs depend on the type used. DWNTs and MWNTs are more readily available and less expensive than SWNTs generally [6].

Despite the distinctive properties of CNTs, the weak interface between nanotubes and the host phase, or "matrix," as well as the difficulty in uniformly

dispersing the CNTs, results in composites that are frequently not as useful as expected. The compatibility of the CNTs and matrix is important. This compatibility is dependent on the bonding between the CNTs and matrix. Another issue that has taken interest is the surface functionalization of CNTs. This approach involves the addition of polar molecules to the surface of CNTs, with the goal of enhancing chemical bonding with the matrix at the interface. One of the first methodical experimental works that focused on the interfacial interaction of SWNT/epoxy-nanocomposites was performed by Cooper et al. [7]. It was reported that the high values of interfacial and breaking strengths were a result of the substantial adhesion between the SWNTs and the epoxy resin matrix.

The effect of particle size has been studied, concluding that composite tensile strength and modulus can be enhanced with decreasing particle sizes at the nanoscale [8]. However, due to the difficulty of obtaining uniform dispersion of nanoparticles at higher particle loading, composites with higher nanoparticle volume percent often result in lower tensile strength than composites fabricated with well dispersed microparticles. This chapter focuses on the background of CNTs and interactions at the interface.

1.1 Carbon Nanotubes

The synthesis of carbon nanotubes evolved from the research on fullerenes [3]. Fullerenes are geometric cage-like structures of carbon atoms that are composed of hexagonal and pentagonal faces. The C_{60} molecule, also

known as Buckminsterfullerene or a Buckyball, was the first closed convex structure form of carbon. The Buckminsterfullerene can be visualized as a soccer ball with 60 carbon atoms arranged where each vertex of a pentagon meets the vertex on the adjacent hexagon. This cage-like structure is symmetrical which results in exceptional material properties such as high elastic modulus and strengths. Fig. 1 illustrates the structure of a C_{60} molecule.

Buckyballs are roughly spherical in shape, while nanotubes are cylindrical where each end is capped. Carbon nanotubes can be envisioned as a sheet of graphite (graphene) that has been rolled into a tube as shown in Fig. 2. Graphene is a 2-D sheet of carbon atoms arranged in hexagonal arrays. In this arrangement, each carbon atom has three neighbors. Rolling sheets of graphene into cylinders form carbon nanotubes. The atomic arrangement (how the graphite sheets are rolled) affects the nanotube properties and nano structure, such as the morphology, diameter, and length of the tubes [3].

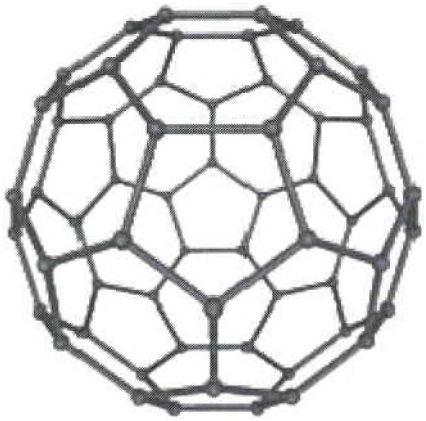

Fig. 1: Fullerene, C_{60} buckyball [9]

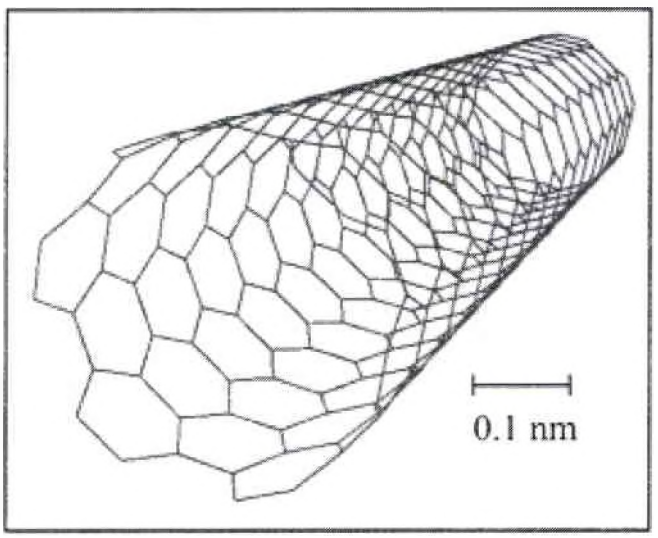

Fig. 2: Illustration of carbon nanotube [10].

There are generally two classes of carbon nanotubes: Single-walled nanotubes (SWNTs) and Multi-walled nanotubes (MWNTs). SWNTs have a diameter close to 1 nm with a tube length that can be many thousands of times longer [11]. SWNTs have larger aspect ratios compared to MWNTs [12]. The specific surface area (SSA) of CNTs is dependent on the diameter and number of sidewalls, where a maximum is achieved with SWNTs. However, SWNTs have a tendency to minimize SSA by forming "ropes" of aligned CNT bundles that are bonded by van der Waals forces [3, 14]. These ropes consist of ten to hundreds of individual tubes that are difficult to separate and infiltrate with a matrix [12]. Furthermore, the ropes can entangle with each other like a ball of string, making it even more difficult to separate and disperse into a polymer

matrix. Fig. 3 shows an example of a SWNT bundle and cross section. The SWNTs can be observed as having the same orientation within a bundle.

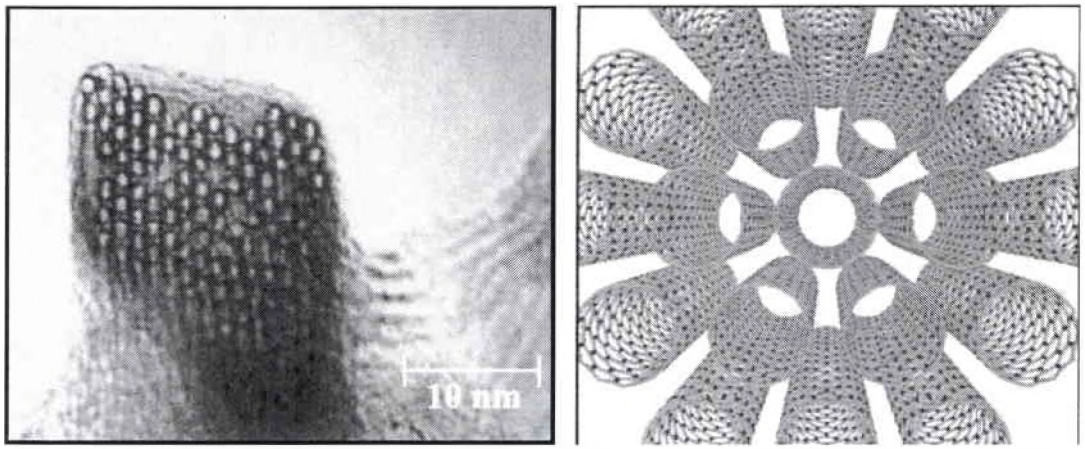

a b

Fig. 3: a) Typical nanotube bundle; b) nanotube bundle cross section [10].

MWNTs consist of multiple layers of graphite rolled in on themselves to form a concentric tube shape. A MWNT can be regarded as nested SWNTs as shown in Fig. 4 [15].

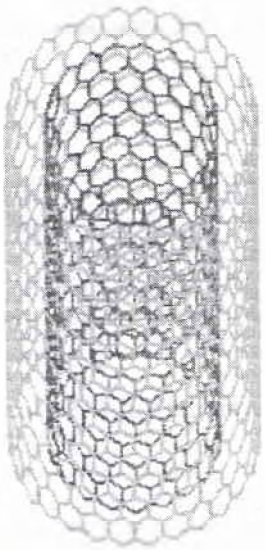

Fig. 4: A multi-walled carbon nanotube.

Because MWNTs have larger diameters than SWNTs and consist of numerous concentric walls, they provide a specific surface area (SSA) of 200 m^2/g or less. Therefore, MWNTs demonstrate better dispersibility, but provide a smaller interface for stress transfer and a lower aspect ratio. The stress transfer between the concentric layers must occur through interlayer shearing to be transferred by van der Waals forces, an attraction force or a repulsion force, all of which are relatively weak [12, 15]. In epoxy matrix composites, MWNTs are considered to be less effective as mechanical reinforcements than SWNTs.

The atomic structure of nanotubes can be described in terms of the tube chirality or helicity that is characterized by the chiral vector, C_h, and the chiral angle, θ. Fig. 5 illustrates cutting the graphite sheet along the dotted lines and rolling the tube so that the tip of the chiral vector touches its tail.

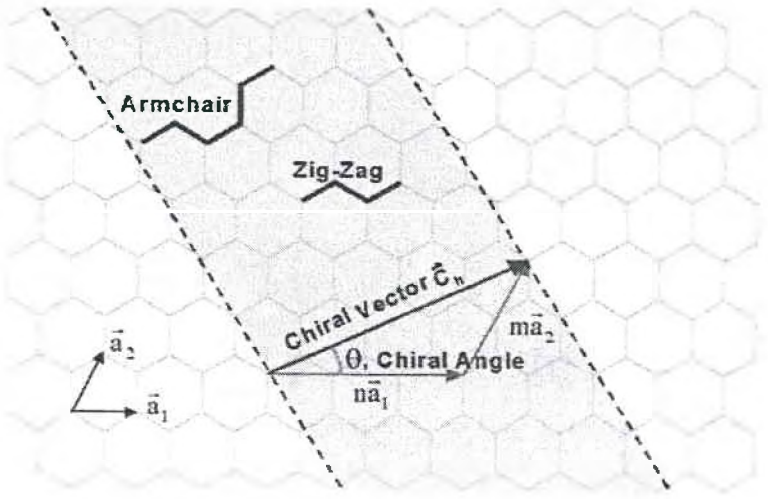

Fig. 5: Schematic diagram of a hexagonal sheet of graphite rolled to form a carbon nanotube [3].

Equation 1 describes the chiral vector, $\mathbf{C_h}$, also known as the roll-up vector where the integers (n, m) are the number of steps along the zig-zag carbon bonds of the hexagonal lattice and $\mathbf{a_1}$ and $\mathbf{a_2}$ are unit vectors [3, 15].

$$\mathbf{C_h} = n\mathbf{a_1} + m\mathbf{a_2} \qquad (1)$$

The chiral angle determines the amount of twist in the tube. There are two limiting cases: at 0° and 30°. These cases are the zig-zag (0°) and armchair (30°). The geometry orientation describes the carbon bonds around the circumference of the nanotube. The index (n, 0) indicates zig-zag type nanotubes and (n, n) for armchair type nanotubes. Fig. 6 illustrates the atomic structure of an armchair and a zig-zag nanotube. Since the nested layers are

structurally independent of one another, the chirality of the layers may be different in MWNTs. The nanotube diameter is also determined by the roll-up vector since the inter-atomic spacing of the carbon atoms is known.

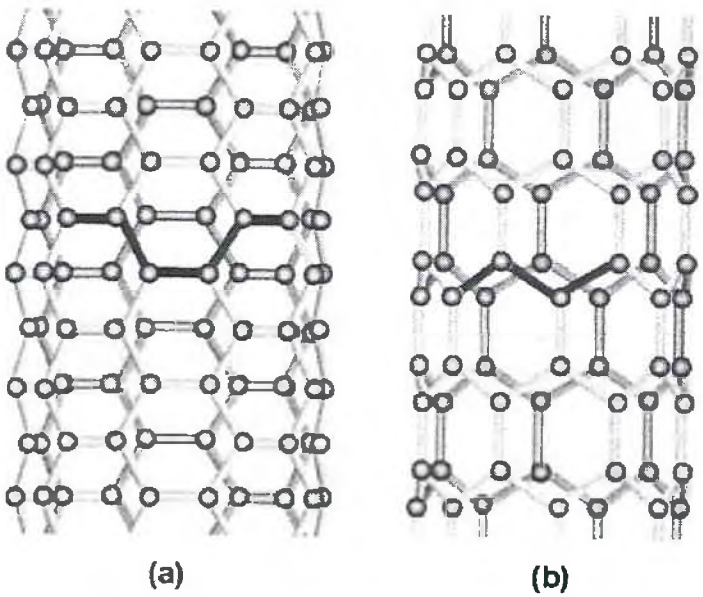

Fig. 6: Illustrations of the atomic structure of a) an armchair and b) a zig-zag nanotube.

The influence of chirality on nanotube mechanical properties has been reported [3]. CNTs instability beyond linear response was analyzed. It was shown that CNTs exhibit outstanding elasticity, sustaining extreme strain without showing any evidence of plasticity or brittleness. The chirality has little influence on the elastic stiffness. A Stone-Wales transformation plays a key role in the nanotube plastic deformation under tension. A set of four hexagonal units is

converted to a structure of two pentagons and two heptagons in pairs (see Fig. 7). This transformation can happen when an armchair nanotube is stressed in the axial direction, which results in ductile fracture for armchair nanotubes.

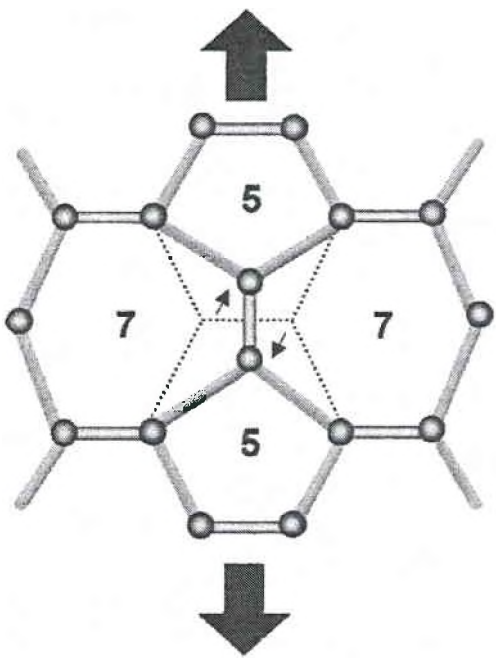

Fig. 7: Stone-Wales transformation occurring in an armchair nanotube under axial tension [3].

The heptagon in the Stone-Wales transformation creates a new defect in the nanotube structure. Heptagons allow for concave areas within the nanotubes [3]. Because of these defects in the nanotubes, countless equilibrium shapes are formed thus leading to plastic deformation.

1.2 Carbon Nanofibers

Another type of carbon nanotube is referred to as a carbon nanofiber (CNF) because its characteristics are different from SWNTs and MWNTs in the following respects: CNFs have a larger diameter (60-150 nm), are longer in length (30-100 micrometers), and have a different wall structure [24, 25]. These materials were developed by Applied Sciences Inc. (Cedarville, Ohio) and are currently manufactured by Pyrograf Products Inc. (Cedarville, Ohio) under the commercial name Pyrograf®-III. They are manufactured in a continuous, vapor phase growth process that contributes to a significantly lower cost (~ $100/lb) than SWNTs and MWNTs, and they are readily available in large quantities. Currently there is capacity to produce 70,000 pounds of CNFs per year. They are also referred to as Vapor-Grown Carbon Nanofibers (VGCF).

Although their intrinsic mechanical properties are not quite as impressive as SWNTs, they provide potential low cost alternatives for achieving considerable improvements in the modulus and strength characteristics of polymer composites, and allowing for easy fabrication of nanocomposite structures by various conventional molding processes. The microstructure of as-received Pyrograf III is comprised of nanofiber agglomerates of 20-100 μm in diameter as well as some de-nested material. Closer examination using TEM indicates that there are several different nanofiber structures possible, such as straight, bamboo, stacked cup, helical, and spherical [26]. A good review of the fabrication and properties of polymer nanocomposites fabricated from CNFs is given elsewhere [6].

1.3 Nanoparticle Dispersion Methods

The fabrication of nanocomposites involves dispersing either single-walled nanotubes (SWNT), multi-walled nanotubes (MWNT), or nanofibers into various polymer matrices in order to take advantage of their superior mechanical and/or electrical properties [2, 3, 6, 12, 16]. With proper dispersion, carbon nanotubes and nanofibers are predicted to provide exceptional material performance improvements. Nanoscale-level dispersion is one of the key challenges in achieving the full potential of these nanoparticles [8]. Examples of techniques used to disperse nanotubes/fibers in polymer resins include one, or a combination of the following: magnetic stir bar mixing, shear mixing, sonication, calendering, use of aqueous ionic surfactants such as sodium dodecyl sulfate, nonionic surfactants, polyelectrolyte "wraps," solvents such as ethanol, acetone, and dimethyl formamide, acids such as hot nitric acid, and dispersion via surface treatments that functionalize the nanotubes [13]. Most of these methods are either not powerful enough to separate agglomerates into individual nanotubes or limited in capacity.

Despite the progress made in this area over the past several years, it is still difficult to ensure the uniform dispersion of carbon nanotubes in a polymer matrix [16]. Five challenges must be overcome in order for CNTs to be effectively distributed: maintaining length of the tubes, reducing or eliminating entanglement, overcoming tube/tube attraction, high CNT loading, and dealing with high matrix viscosity that results from nanotube addition. Other critical

barriers to the wide-spread use of nanotubes are poor nanotube-matrix adhesion, high cost, and short supply of nanotubes, especially SWNTs.

Three dispersion methods are further described in this chapter: sonication, mechanical agitation and calendering.

1.3.1 Sonication

Ultrasonic devices (baths or horn-type probes) are ideal for preparing small batches of low viscosity matrix materials. Due to the tremendous reduction of the vibrational energy with increasing distance from the sonotrode, large batches are not practical [12]. Agglomerates and individual CNTs experience rupture and damage as well as reduced aspect ratio as a consequence of the local energy input. In order to produce CNT-nanocomposites, the sonication technique is best applied by first dispersing CNTs into an appropriate solvent (e.g. ethanol, acetone) [16]. The solvent permits the agglomerates to be separated due to the vibrational energy at the micron level. The suspension can then be combined with the epoxy, followed by solvent removal via evaporation. Fig. 8 illustrates agglomerates remaining after MWCNT/epoxy resin was sonicated. Overall, this is not the most efficient dispersion process.

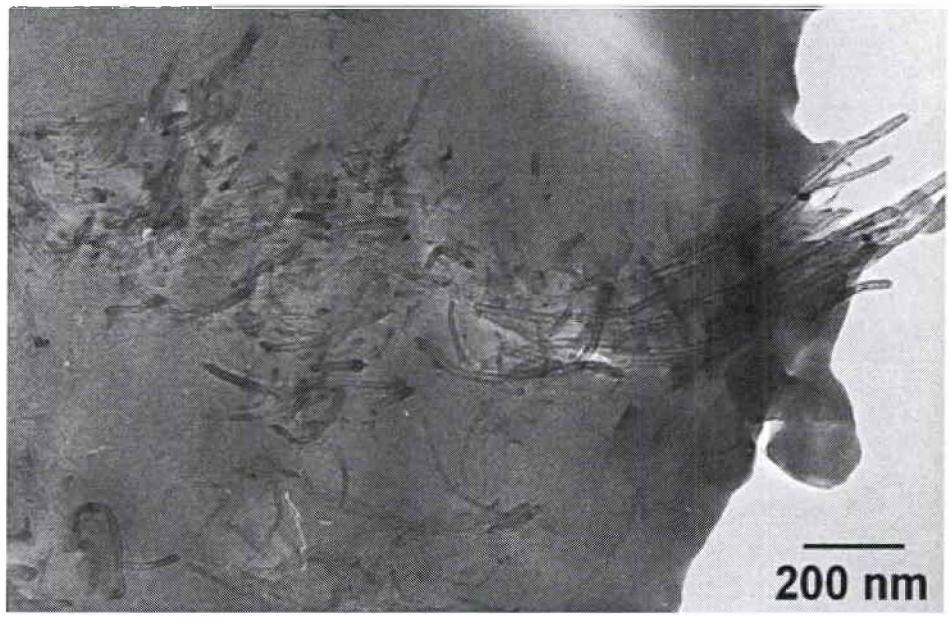

Fig. 8: Typical TEM micrograph of sonicated MWCNT/epoxy composite [16].

1.3.2 Mechanical Agitation

The effectiveness of dispersing nanotubes by stirring is dependent on the size and shape of the propeller and mixing speed [16]. High shear rotor-stator emulsifying units are often used [26]. Some reports claim that MWNTs were satisfactory dispersed in epoxy resin as a result of intensive stirring. MWNTs are generally easier to disperse in epoxy than SWNTs but often tend to re-agglomerate. Frictional contacts and elastic interlocking mechanisms cause this flocculation behavior [16]. Additional parameters such as weak attractive forces and sliding forces minimally contribute to flocculation during stirring.

1.3.3 Calendering

Calendering is another method to achieve particle dispersion. It also has the potential to scale-up batches to satisfy industrial demands, especially in

thermoset and elastomer applications. Calendering was historically used to disperse micro-particles in different matrixes, (e.g. color pigments for paints and cosmetics). Shearing is the main mechanism that contributes to efficient dispersion and manufacturing of large batches of nanocomposites using this technique. Fig. 9a illustrates the configuration of a three roll mill that consists of three adjacent cylindrical rolls, where each turns at a different velocity. The first and third rolls (feed and apron) rotate in the same direction while the center rotates in the opposite direction. High shear rates in the fluid form due to the narrow gap between the rolls, δ_g, combined with the mismatch in angular velocity of the neighboring rolls, $\omega_1 < \omega_2 < \omega_3$. Fig. 9b shows the area of intense shear mixing between the adjacent cylinders. The gap setting (δ_g), can be adjusted as low as 5 μm to 100 μm.

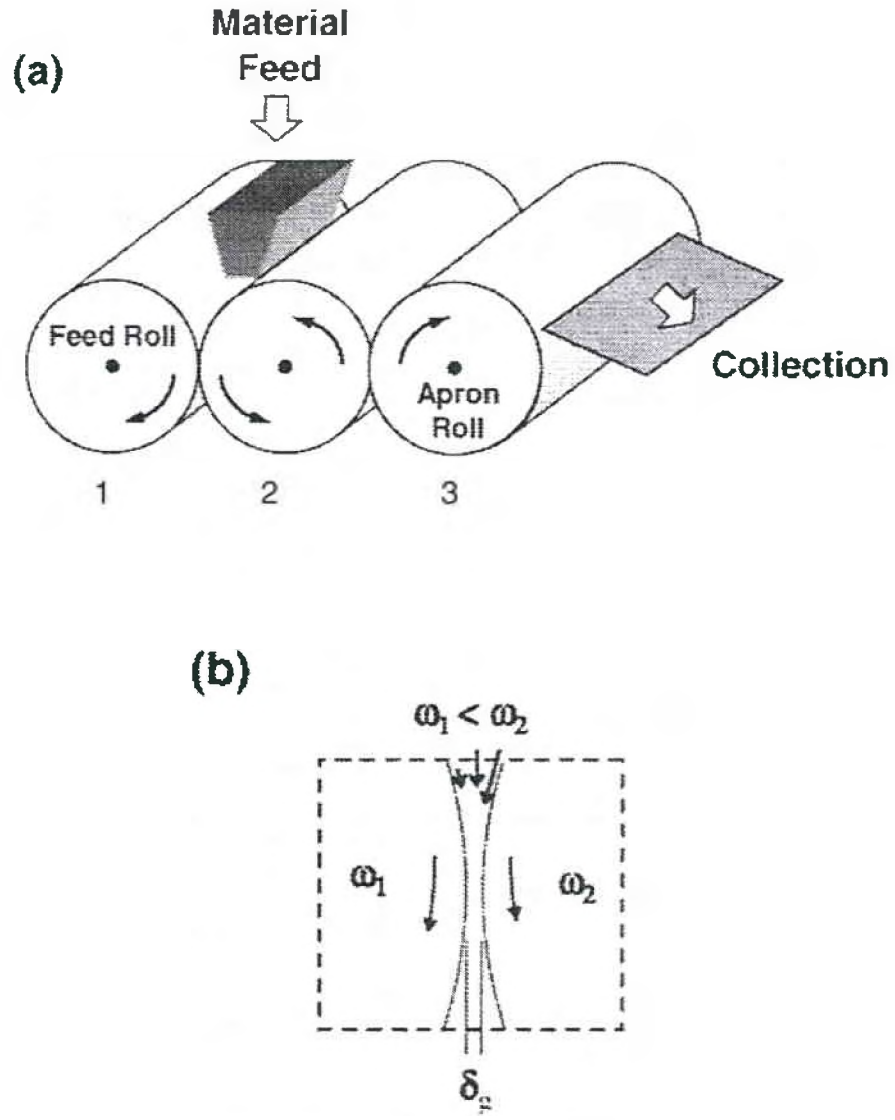

Fig. 9: a) Schematic diagram showing the general configuration of a three roll mill; b) region of high shear mixing between the feed and center rolls [2].

Because calendering uses high shear forces in a short residence time, the breakage of individual CNTs is limited, while nanotube agglomerates are broken and untangled.

Fig. 10 illustrates the progressive development of nanocomposite structure during the calendering process. Fig. 10a displays a highly agglomerated CNT/epoxy mixture at a gap setting of 50 μm. Many agglomerated CNTs were observed, and only a minute fraction of individual CNTs actually dispersed in the matrix. Fig. 10b shows the structure of the nanocomposite after processing at 20 μm gap. The majority of the agglomerates are on the order of a few microns diameter. In Fig. 10c, the agglomerate size is in the micron or submicron range after milling with a gap setting of 10 μm. Fig. 10d illustrates that at a gap setting of 5 μm a highly dispersed nanocomposite with little or no agglomerates is observed. It was concluded that after processing at increasingly smaller gap settings, a greater quantity of CNTs are dispersed in the matrix with smaller agglomerate sizes.

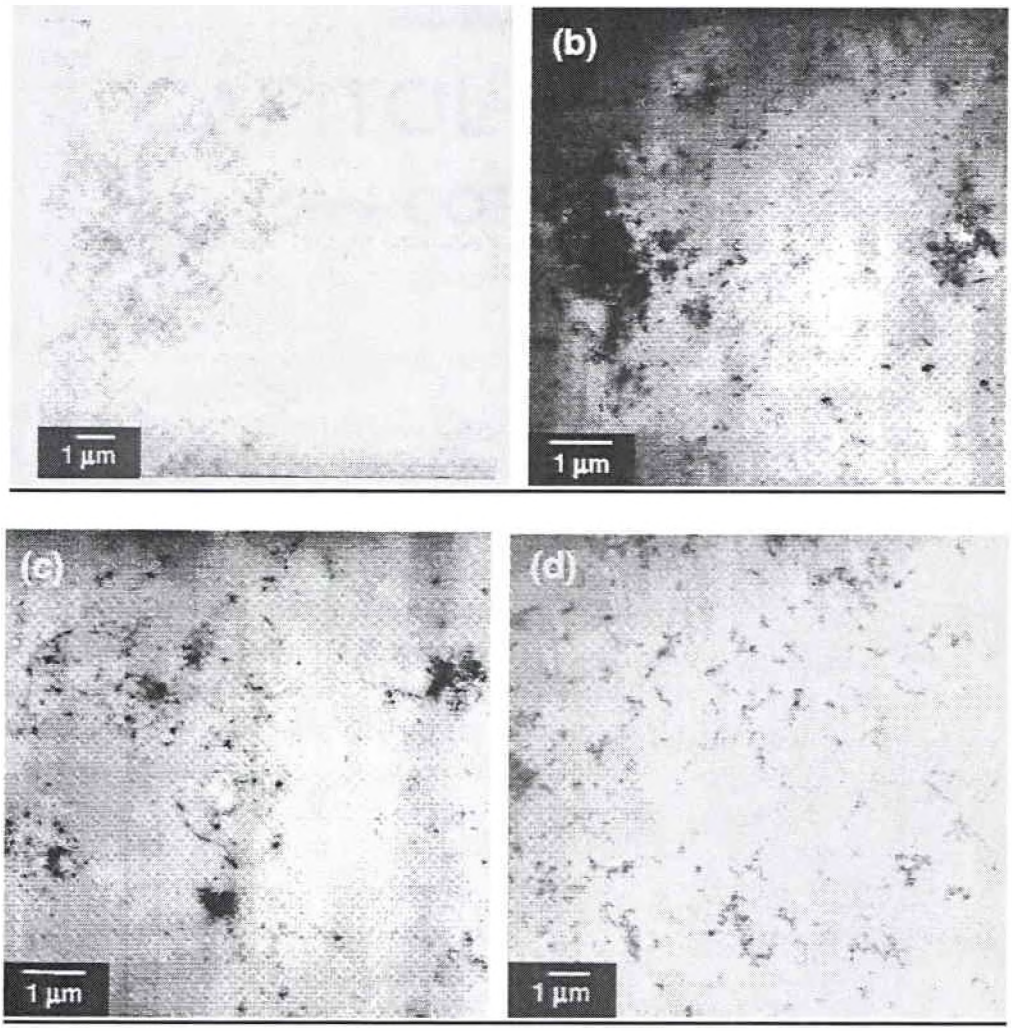

Fig. 10: CNT/epoxy nanocomposite structure development after processing at different gap settings: a) 50 µm; b) 20 µm; c) 10 µm; d) 5 µm [2].

1.4 Interfacial Adhesion

A critical issue when processing nanocomposites is interfacial adhesion between the matrix polymer and nanotube. The interface must be strong enough to transmit the stress due to a mechanical load from one phase to the other [17]. Without this bond, the dispersed phase (CNTs) fails to connect with the matrix. This defect undermines the purpose of adding CNTs as a structural

reinforcement. Because nanotubes tend to slip when assembled in ropes or agglomerates, thus reducing the interfacial bonding to the matrix, ropes and aggregates reduce the effective aspect ratio of the reinforcement. With an absence of a chemical bond between the matrix and CNT, an interfacial shear stress can separate the matrix from the reinforcement [18]. Fig. 11 illustrates the contrasting microstructures of poorly bonded and well-bonded interfaces in a fiberglass composite. In Fig. 11a, the fibers are clearly separated from the surrounding matrix, while in Fig. 11b the matrix is clearly bonded to the fiber, and the matrix fracture is more pronounced near the fiber surface.

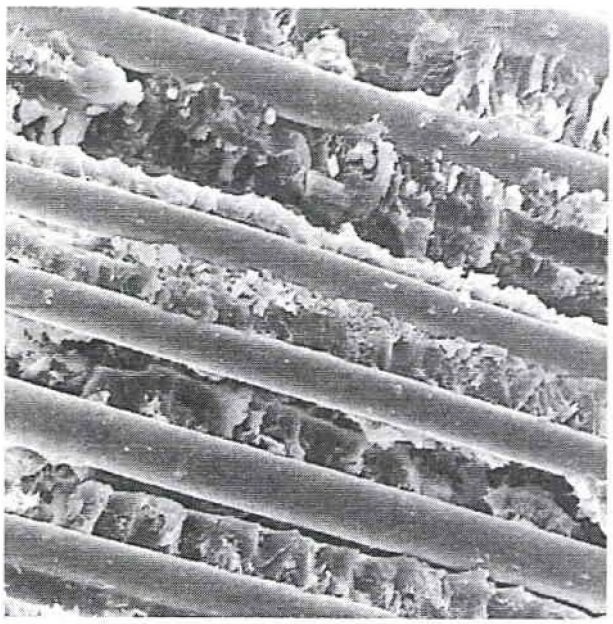

(a)

(b)

Fig. 11: SEM image of fracture surface of epoxy-fiberglass laminate illustrating a) poor bonding interface; b) well-bonded interface [18].

Potential methods to improve the interfacial bonding include physical and chemical surface treatment. Research has shown that the interfacial bonding between the CNTs and matrix can be improved by chemically functionalizing the CNT surface [12]. The introduction of customized chemical groups (e.g. amino-, carboxyl-, or glycidyl-groups for epoxies) enables covalent bonding between CNTs and epoxy, improves the interfacial stress transfer, and positively affects the dispersibility of the nanofiller.

1.5 Problem Statement

The goal of the present study is to document the mechanical, physical, impact, and morphological properties of epoxy nanocomposites formed from a variety of functionalized and nonfunctionalized carbon nanofibers and carbon nanotubes, and determine their effect on improving resin properties. A simple dispersion process was used to disperse this wide variety of nanoparticles into a model epoxy-amine resin system. Furthermore, a simple approach for forming films of the uncured nano-modified resin, and producing composite laminates through Resin Film Interleaving was demonstrated, and composite impact properties evaluated. Relative to previous related thesis work at the University of Dayton, this thesis involves several new developments, including use of a solventless dispersion process, oxidized nanofibers and nanotubes, a new mixed SWNT/MWNT raw material referred to as "XD", new analytical techniques, and the use of impact strength tests.

CHAPTER 2

LITERATURE REVIEW

Carbon Nanotube Functionalization and Composite Characterization

The approach of treating carbon nanotubes (CNTs) to enhance their compatibility with a polymeric matrix has been previously explored. The goal of chemical modification or functionalization of SWNTs and MWNTs is to bond nanotubes directly to the matrix [1, 19]. This linkage can be achieved by a reaction of functional groups on the nanotubes with those of the matrix, which enables a stress transfer between the nanotubes and the polymer. The result should be improved mechanical properties. It was predicted and confirmed by calculations that functionalization of less than 1% would improve interactions between nanotubes and the polymer without considerably decreasing CNTs strength [1]. Two methods for functionalizing a CNT surface have been developed: direct addition to the graphitic nanotube wall, and functionalization at defect sites [19]. The latter takes advantage of organic groups such as carboxylic acids at the defect sites.

The most logical approach to develop polymeric carbon nanocomposites is to functionalize CNTs with organic groups or polymers that are structurally similar to the matrix polymer. Otherwise the species used in the functionalization

of CNTs become "impurities" in the final nanocomposite. A few examples that have been tried are as follows: Octadecylamine-functionalized SWNTs were dispersed into a polypropylene matrix via a solution-based technique that took advantage of the shared solubility of the functionalized nanotube and the matrix polymer in the same select solvent [19]. Another example involved functionalizing CNTs through the covalent attachment of polystyrene copolymers, and then dispersing the polystyrene copolymer-functionalized CNTs into the polystyrene matrix to fabricate nanocomposite thin films. Fig. 12 illustrates a plausible functionalization process of CNTs, from oxidation to the composite manufacturing.

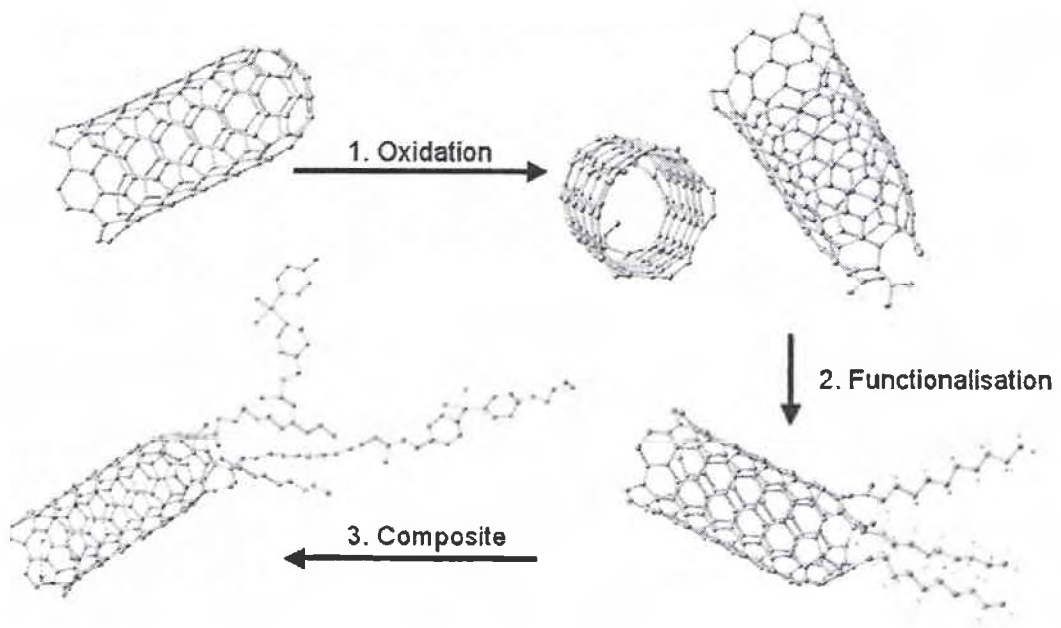

Fig. 12: Functionalization process of CNTs: 1) nanotube ends are oxidized; 2) functionalized to form an end group; 3) finally processed to the nanocomposite and reacted with the matrix [16].

Another method to integrate CNTs into the matrix is the use of surfactants, [16] which coat the individual nanotubes and form a physical bridge to the matrix. The benefit of this procedure is that physical adhesion does not degrade the structural quality of CNTs, whereas a covalent attachment of functional groups always disrupts the graphene layers of the nanotube.

2.1 Types of CNTs Functionalized End Groups

Several approaches have been employed to control the optimum amount and type of functionality on CNTs. These techniques involve various parameters such as: solvent selection, sonication, filtration, and vacuum drying. Four types of CNT functionalization methods will be discussed.

2.1.1 Esterification of Poly(vinyl alcohol) (PVA)and Oxidized CNTs

Covalent attachment of PVA to nanotubes has been used to enhance the wet-casting of nanocomposite thin films. The process involves reacting PVA with carboxylic acid groups that are attached to the surface of the nanotubes. The reaction is activated by the addition of carbodiimide, which is a functional group consisting of the formula N=C=N. Both SWNTs and MWNTs can be functionalized using this method. Fig. 13 shows this scheme. Purified SWNTs were added to a mixture of N,N-Dicyclo- hexylcarbodiimide, 4-(dimethylamino)pyridine, 1-hydroxybenzotriazole, and dimethyl sulfoxide (DMSO) and sonicated. Next, a solution of PVA in DMSO was added, sonicated and centrifuged at high speed. The results showed that functionalized CNTs

improved the optical quality of the PVA-CNTs nanocomposite thin films without any observable phase separation [19].

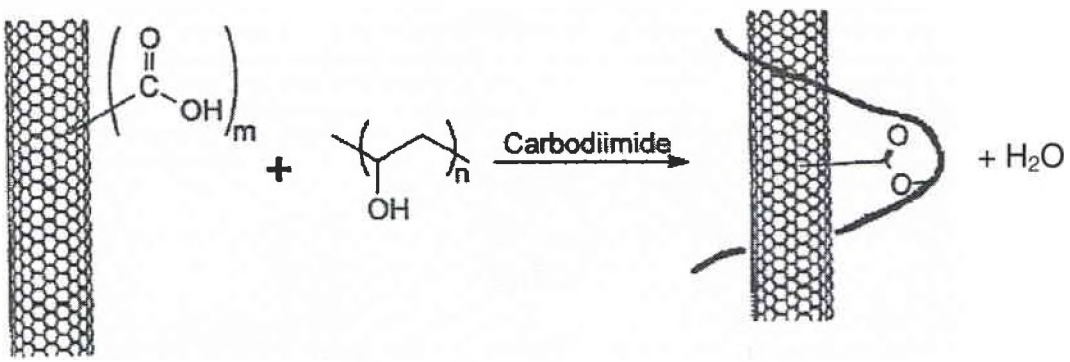

Fig. 13: Functionalization of SWNTs and MWNTs via PVA in carbodiimide-activated esterification reactions [19].

2.1.2 Oxidation with Nitric Acid

Researchers have demonstrated that Vapor Grown Carbon Nanofibers (VGCF) oxidized to low oxygen concentrations by soaking in nitric acid improves tensile strengths of a wide variety of polymers such as polypropylene and epoxy [6]. In one study, VGCF were etched in air near 400°C, and then soaked in sulfuric/nitric acid mixtures. This treatment covered one fourth of the fiber's surface with oxygen atoms [6]. In another study, the fibers were more dispersible in water due to the fiber surface covered with micropores, which resulted up to 22% surface oxygen coverage [6].

In the case of polypropylene composites, only modest surface oxidations (up to 4% surface oxygen atoms) produced composites with the optimum tensile strengths. Composite tensile strength decreased with increased oxygen

concentration. Conversely, epoxy composite tensile properties improved with highly oxidized nanofiber surfaces. It was reported that a 35% strength improvement and a 140% modulus improvement was observed with a 4 wt% loading of highly oxidized VGCF [12].

2.1.3 Oxo-fluorination of CNTs

The effects of oxo-fluorination of CNTs have been investigated for SWNTs and MWNTs. This process involves epoxy-based nanocomposites containing fluorinated SWNTs experienced an increase in the modulus, but a linear decrease in the glass transition temperature with increasing filler content [12]. It was concluded that fluorination of SWNTs should not be considered for substantially improving the interfacial adhesion. In another study, however, the fracture toughness of epoxy nanocomposites containing oxo-fluorinated MWNTs was improved [12]. It was concluded in this study that the bonding to the matrix was improved by polar interactions as a result of the modified surface polarity of the CNTs. This fluorination produces additional hydroxyl groups on the CNT surface enabling hydrogen bonds to the matrix.

2.1.4 Alkylamino-functionalized SWNTs

Carboxylic groups can be added to the surface of a carbon nanotube via an oxidative treatment. This functional group results in an opening of the CNT end cap [16]. This can permit direct bonding of the tube ends via the carboxylic groups to the matrix. The next step involves reacting carboxylic groups with

multifunctional amines. When the amino-functionalized nanotubes are added to epoxy, the free amino groups on the surface of the CNTs will react with the epoxy molecules forming covalent bonds that are equivalent to the normal epoxy-amine polymer bond. Epoxy nanocomposites experienced increased glass transition temperature and improvement in strength and modulus when alkylamino-functionalized SWNTs were used. These functionalized CNTs also enhanced dispersion and adhesion to the matrix at loadings as little as 1 wt%. As a result of covalent bonding generated, SWNTs were incorporated directly into the epoxy network.

2.2 Composite Characterization

There have been significant challenges in the micromechanical characterization of nanotubes, as well as the modeling of elastic and fracture behavior at the nanoscale [3]. The challenges in the characterization of nanotubes and their composites include a lack of micromechanical characterization techniques for direct property measurement, uncertainty in data obtained from indirect measurements, insufficient test specimen preparation techniques, and lack of control in nanotube alignment and distribution.

The elastic modulus of nanotubes has been measured with an atomic force microscope. This direct measurement of the stiffness and strength quantifies the bending force as a function of displacement along the unpinned length of the nanotube [3]. In contrast, several techniques have been used successfully to characterize the bulk mechanical properties of nanocomposites.

For example, methods to determine fracture toughness include Single-edge-notch bending (SENB), IZOD impact strength, three point flexure testing, and compact tension [2, 12]. In addition, thermal conductivity (k) can be measured by the flash diffusivity technique. The following equation describes this relation:

$$k = \alpha \rho C_p \quad (2)$$

where α is the measured thermal diffusivity, ρ is the density, and C_p is the specific heat [2]. Electron microscopy (EM) has been used to analyze nanotubes and nanocomposite morphology at higher magnifications than possible with optical microscopy. The most used EM methods are Scanning Electron Microscopy (SEM) and Transmission Electron Microscopy (TEM).

The two mechanical properties that will be further discussed are fracture toughness and nanotube buckling.

2.2.1 Fracture Toughness

Epoxy resins are the most widely used thermoset matrix for various composite and adhesive applications [12]. They possess high strength and stiffness, good thermal and thermo-mechanical stability, excellent chemical resistance, but relatively low toughness. The fracture strength or "toughness" of materials correlates with increased resistivity against initiation and propagation of microscopic cracks that could ultimately lead to failure. Since fracture strength is a direct measurement of damage tolerance, it is essential for the design of

structural components, especially with respect to the long-term fatigue behavior. The most essential micro-mechanical mechanisms leading to an increase in fracture toughness of composites are: (i) localized plastic deformation and void nucleation, (ii) particle or fiber debonding from the matrix, (iii) crack deflection, (iv) crack pinning, (v) fiber pull-out, (vi) crack tip deformation, and (vii) particle/fiber deformation or breaking at the crack tip [12, 16]. The overall size of the plastic deformation zone is also a factor. These mechanisms are affected by numerous factors such as reinforcement particle size and shape, particle-matrix interfacial adhesion values, volume fraction of particles, and others, which are frequently complicated to differentiate.

Debonding initiation usually occurs at one pole of the particle that lies in the axis of the applied tension [8]. The debonded area and the number of debonded particles multiply as the applied stress increases.

Thermosetting polymers have a superior resistance to plastic deformation because of their crosslinked molecular network. Rigid particles can stimulate shear yielding in epoxy by aiding a change in stress state, e.g. from plane strain to plane stress conditions [20]. This may be a consequence of voids, cavities, and debonding effects in the crack tip's process zone. The size of this zone can be defined as a plastic zone. Equation 3 calculates the zone's radius, r_p, and diameter ($2r_p$), which depends on the static fracture toughness, K_{Ic}, and the yield strength, σ_y, of the polymer matrix [20]:

$$2r_p = \frac{1}{3\pi}\left(\frac{K_{Ic}}{\sigma_y}\right)^2 \qquad (3)$$

Overall, the size of the plastic zone of brittle epoxy is relatively small. For example, in a composite with microparticles, only a negligible amount occupies the plastic zone deformation process [16]. However, when nanoparticles are incorporated in the resin, a substantial amount of particles can occupy the plastic zone.

Composites that contain nanoparticles have been observed to experience substantial improvement in fracture toughness [16]. Even nonfunctionalized nanoparticles have been observed to increase the fracture toughness of the epoxy matrix at low levels [12]. All nanocomposites contain at least a small fraction of partially agglomerated CNTs. Interestingly, void nucleation, crack deflection, and localized inelastic matrix deformation were observed at these agglomerates [12, 16]. Tail-like structures form on the fracture surface, which show the CNTs interacting with the crack path and therefore results in crack deflection. Improvement of fracture toughness is dependent on a large interfacial area of reinforcement. However, the fracture toughness decreased at higher filler contents, which was attributed to excessive agglomeration.

Amino-functionalized CNTs have been confirmed to outperform nonfunctionalized CNTs when dispersed in epoxy resin [16]. This was attributed to increased interfacial adhesion and the superior dispersibility that gives a more homogeneous distribution in the matrix and reduced agglomerates. However, if the interfacial adhesion is excessively strong, generally the composite toughness can be decreased by suppressing interfacial failure [12].

2.2.2 CNT Buckling

Buckling and compressive deformation of CNTs have been the subject of several experimental and computational studies. Buckling is reported to be influenced by the forces exerted in the fiber-matrix interfacial region as well as the elastic properties of the matrix immediately surrounding the fiber [21]. The Brazier effect, nonlinear flattening of elastic tubes under bending, has been used to describe the cause of CNTs' circular cross-section becoming more uniformly 'ovalized' along the entire tube length as the bending curvature increases [22, 23]. In compression, CNTs have demonstrated tremendous mechanical flexibility. It has been shown that kinking and bending of CNTs are reversible up to large bend angles (e.g. ~180°) without experiencing catastrophic fracture [4, 22].

The buckling behavior of MWNTs in a nanocomposite material varies with the nanotube diameter. It has been reported that smaller diameter CNTs deform through global bending of the nanotube in a manner analogous to Euler-type bucking modes where the overall nanotube is curved when deformed in compression [4]. Bending of MWNTs requires displacement of all the nanotube walls. Therefore, the additional nanotube walls and larger tube diameters will produce higher flexural stiffness, which leads to increased resistance to buckling.

When the nanocomposite deforms in compression, the polymer matrix supports the nanotube and the overall buckling of the CNT is constrained. Without the matrix restriction, the CNT may develop local kinks in the sidewalls that will enable large-scale bending of CNTs [4]. Continuum-based shell and beam theory have been used to explain this phenomenon. Buckling of fibers in

an elastic medium has been studied for both nonfunctionalized and functionalized interfaces. The critical stress can be calculated to determine the maximum load applied before catastrophic failure. Equation 4 expresses the critical stress (σ_{cr}) of an unfunctionalized SWNT embedded in an elastic medium, where P_{cr} is the critical load, and R and h are the outer diameter and wall thickness of the CNT respectively [21]:

$$\sigma_{cr} = \frac{P_{cr}}{2\pi Rh} \tag{4}$$

Since the force between the fiber and matrix is subject to van der Waals interactions, the lateral displacement due to buckling is small and there is basically no effect on the matrix [21]. The deformation of the matrix as a result of fiber displacement only takes place during the post-buckling phase and does not influence the critical stress for buckling. This continuum model predicts a higher critical stress than that calculated using molecular dynamics simulation. Therefore, molecular scale interactions must be cautiously investigated before using this continuum model.

The critical stress for buckling of functionalized nanotubes is expected to be different than neat nanotubes because of the changes in curvature introduced by chemical bonding. By attaching a hydrocarbon molecule to the sidewall of a nanotube, the graphite bond structure transforms from sp^2 to sp^3. The CNT radius curvature increases when chemical attachments are present. Chemical attachment effectively reduces the total CNT length into smaller subsections,

which increases the critical load for buckling. For this case, continuum theory model is a column subdivided by *n* uniformly spaced inflexible restraints [21]. Equation 5 applies to this system:

$$\sigma_{cr} = \frac{P_{cr}}{A} = n^2 \frac{\pi^2 E}{\left(L/r\right)^2} \tag{5}$$

where A is the area for the spaced restraints, L is the total length of the CNT, E is the elastic modulus, and r is the radius of the CNT. As *n* increases, the continuum theory predicts that the critical stress will increase by n^2 [21]. Conversely, atomistic simulations show that the critical stress for buckling is reduced due to modified CNT surface. However, because the CNTs and matrix are bonded, stress is transferred efficiently to counter failure due to buckling.

It has been observed that chemical attachments between the matrix and CNTs can debond and re-attach with adjoining atoms of nanotubes before complete failure [21]. This behavior is more common in tensile loading, but also occurs in compression loading. At the atomic level, individual bonds in the matrix rotate and realign themselves until the bonds are stretched. Bonding with new sites on the carbon nanotube is a way of reestablishing equilibrium. The CNTs on the other hand are only deformed significantly during the post-buckling stage of loading. The extending of the bonds in chemical attachments and load transfer depends on the density of the chemical attachment, distance between the fiber and matrix, length and type of chemical attachments, etc. At nanoscale

interfaces, all these factors affect the load transfer mechanism and need to be accounted for in continuum or atomistic simulations.

CHAPTER 3

EXPERIMENTAL PROCEDURES

3.1 Sample Fabrication

3.1.1 Raw Materials

The epoxy resin system used in this study was EPON 862/W (Hexion), see Figure 14. This system is comprised of DiGlycidyl Ether of Bisphenol F (DGEBF) at 100 phr and diethylenetoluenediamine (DETDA) at 26.4 phr. The mixed system is a liquid with a viscosity of approximately 4200 cP at room temperature and is widely used in resin transfer molding (RTM) and vacuum assisted RTM (VARTM) processes. It was used in this study because of its low viscosity which makes it easy to process with nanoparticles compared to higher viscosity, toughened aerospace resins. EPON 862/W has been used in numerous studies as a baseline resin for nanocomposite fabrication, therefore a large data base exists in the literature [2, 26, 27].

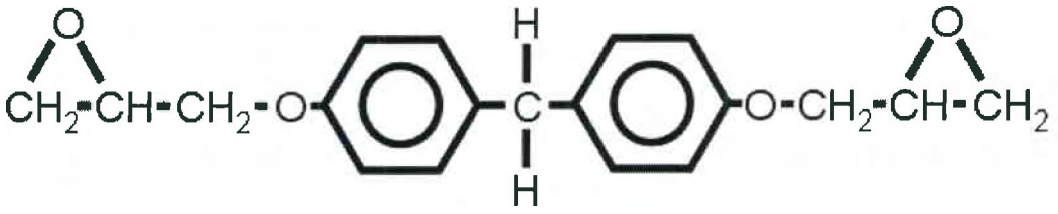

a

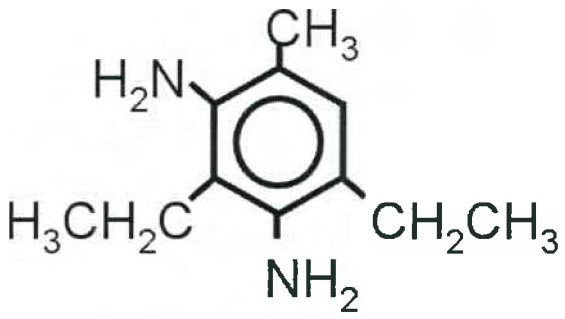

b

Fig. 14: a) EPON 862 structure (DGEBF), b) Epikure W structure [13].

Pyrograf III vapor phase grown carbon nanofibers (VGCF) were obtained from Applied Sciences Inc. (Cedarville, Ohio). This relatively low cost material (~$220/kg) was used early in the research to help debug the various processing steps. Several grades were available, but one was deemed the most suitable for mechanical property improvements. The grade PR-24-LHT-XT has an average diameter of 100 nm and has been heat treated in an inert atmosphere by the manufacturer. The heat treatment helps to clean the nanofiber surface of polyaromatic hydrocarbons and increase the degree of graphitization compared to non-heat treated versions. The microstructure of as-received Pyrograf III material can be seen in Figure 15. It is comprised of nanofiber agglomerates as

well as some de-nested material. Closer examination using TEM (not shown) indicates that there are several different nanofiber structures present, such as straight, bamboo, stacked cup, etc. [26].

Two separate batches of PR-24-L4T-XT were obtained and were labeled in this study as UDRI batch #71 and batch #94. Two samples from each batch were further treated using a scaleable oxidation process at UDRI. Although the details of this process are not presented here, the end result was the covalent attachment of oxygen onto the VGCF surface. A total of 4 batches of oxidized VGCF were produced as illustrated below. Each of these batches, in addition to the two control batches (#71 and #94) were dispersed in EPON 862/W at a loading of 8 wt%.

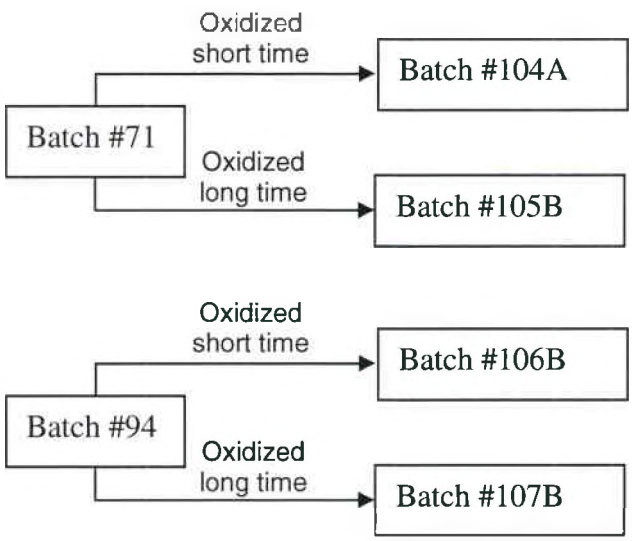

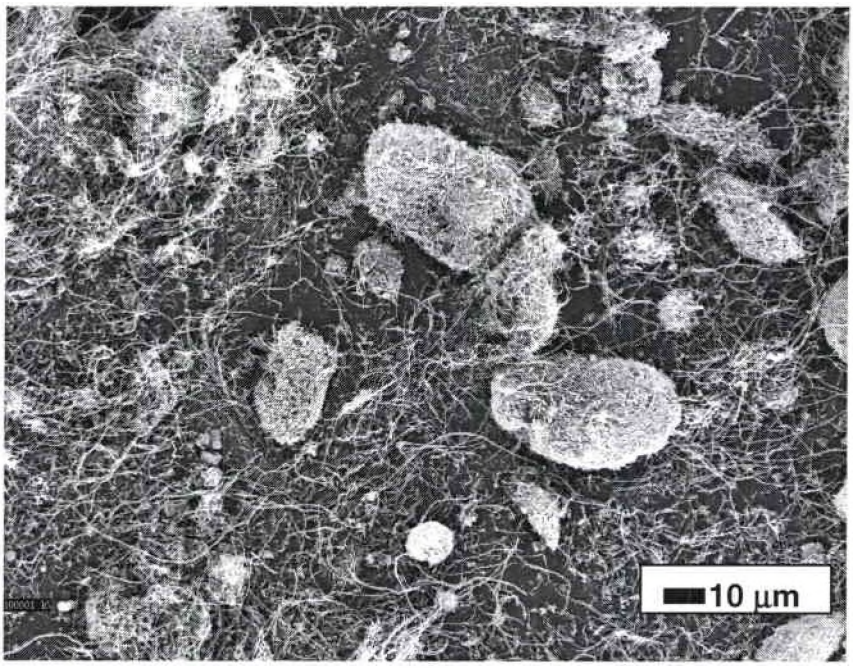

a

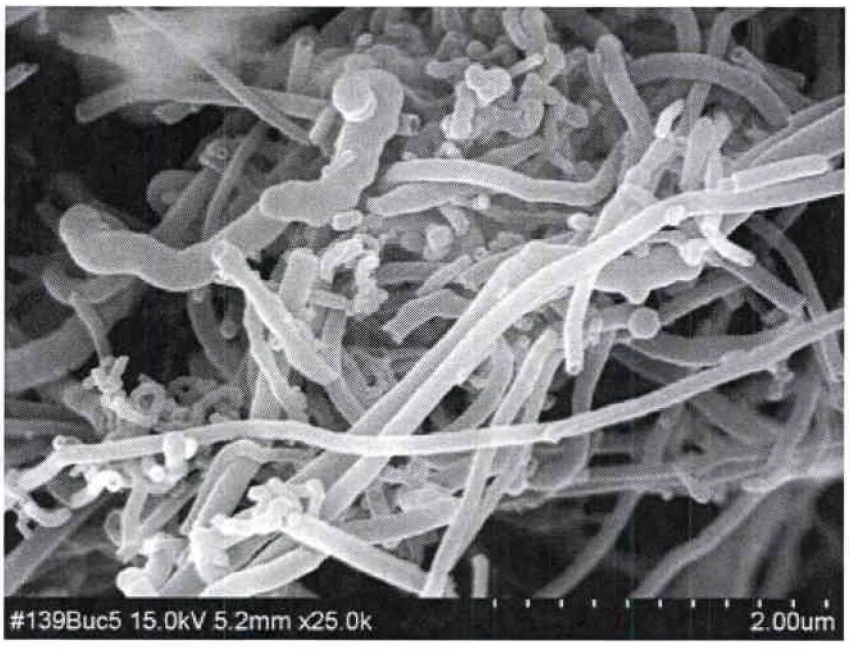

b

Fig. 15: Typical as-received VGCF sample at a) low magnification, showing tightly nested nanofiber agglomerates and some separated nanofibers; b) high magnification, showing distribution of nanofiber diameters.

Single and multiwall CNTs were obtained from CNI (Houston, TX). Since this particular material is experimental, it was provided to this research program at no cost. The grade used, XD3365A, ranged in diameter from 5 nm to approximately 50 μm and was used in the as received state. A sample of XD was also oxidized at UDRI to provide a functionalized material. The CNTs were dispersed in EPON 862/W at loading of 0.15 wt%.

Carbon fiber laminates were produced using unidirectional carbon fiber knitted fabrics. Approximately 1.1 square meters of unidirectional carbon fabric (Hexcel, 290 g/m^2) made from IM7 12k tows unitized with a hot melt yarn was obtained. The material was manually cut with a razor blade into 15 cm x 15 cm squares.

3.1.2 Fabrication of Epoxy Nanocomposites

A solvent-free, high shear melt compounding process was used to disperse the carbon nanofibers and nanotubes in the resin (see Fig. 16). The process, also known as calendering as described in Chapter 2, involves shearing the resin in a small gap between two metal cylinders counter rotating at different speeds [2, 16]. The material is briefly exposed to a zone of high shear rate at the nip between the rollers. This is essentially a batch process, and the equipment, a 4" x 8" calendering roll mill by Keith Machinery Corporation, was suitable for processing 50-500 g of material in this study. Roll speeds were approximately 40, 105, and 270 RPM. A batch size of 200 g (resin + VGCF) for each VGCF type was used, with four passes per batch. Carbon nanofiber loading was

8 wt%. A batch size of 150 g (resin + CNT) for each CNT type was used, and four passes per batch were used as well. The carbon nanotube loading was 0.15 wt%.

The dispersion process first involved hand premixing the nanofibers or nanotubes into the freshly mixed resin system in the proper proportion. For the XD material, some of the batches were mixed into a "chem-staged" epoxy resin system in order to increase the viscosity to provide a higher shear stress during dispersion. Chem-staging is a method of advancing the degree of cure of a thermoset resin to a level between 0% and the gel point. It involves adding only a small fraction (5, 10, or 15% in this study) of the curing agent to the epoxy, heating the mixture through a normal cure cycle to fully react the curing agent, cooling, and then adding the balance of the curing agent for full stoichiometry. This is different than the more well known thermal B-staging approach, in which the full stoichiometric amount of curing agent is added, and the mixture is subject to heating at a temperature lower than the gel temperature. The advantages of chem-staging are more precise control over the advancement of cure and avoiding the over-curing due to an exothermic runaway. In the current study, the nanotubes were added after the chem-staging cycle was complete and the balance of the curing agent was added.

After dispersion, the resulting mixtures were degassed in a Fisher Scientific Isotemp® Vacuum oven at 55°C under a vacuum of absolute pressure of ~ 4.0 in Hg for 10 minutes. The material was then packed into a multicavity silicone rubber mold (Fig. 16b), covered with a rubber sheet, and compressed

and cured into solid plaques using a Tetrahedron programmable flat platen press. The cure cycle was 2 hours at 121°C and 2 hours at 177°C, and pressure 0.687 MPa (100 psi) at all times. Plaques were made with thickness of 6.35 mm (1/4 inch) for flexure testing and 3.175 mm (1/8 inch) for impact testing (Fig. 16).

Both rubber molding and a glass molding technique were used for the XD nanocomposites. In the glass molding method, the nanotube mixture was degassed and cured between two glass plates. This system was comprised of two borosilicate glass plates separated by a silicon rubber gasket of 1/8 or 3/16 of an inch (Fig. 17). The glass plates were prepared by coating the surfaces with 5 coats of a releasing agent, Frekote 44NC, and allowing 10 minutes of drying time between each coat. The glass plates were rotated 90° before applying the next coat. After applying the final coat, the glass plates were placed in an oven for 30 minutes at 55°C to evaporate any remaining solvent. Next, the glass plates were assembled together with the rubber sheet gasket separating them, and secured with binder clips. After curing the nanotube/epoxy mixture, plates were easily separated, and then the release coat was reapplied. The glass plates were offset vertically by ~ ½ inch to allow easy pouring into the cavity. The mold was placed standing up in a Blue M programmable oven and cured for 2 hours at 121°C and 2 hours at 177°C.

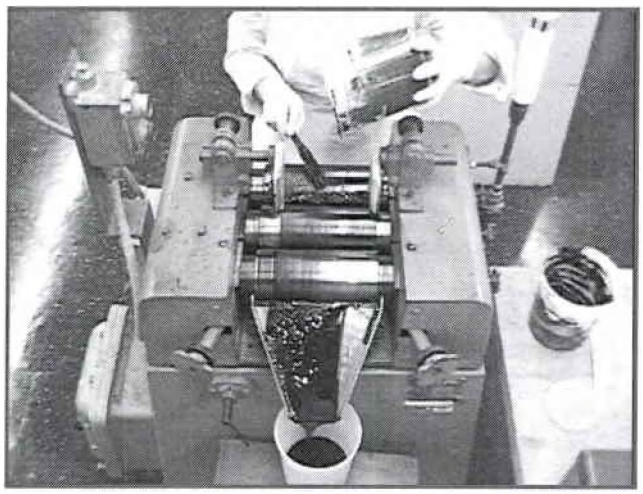

a

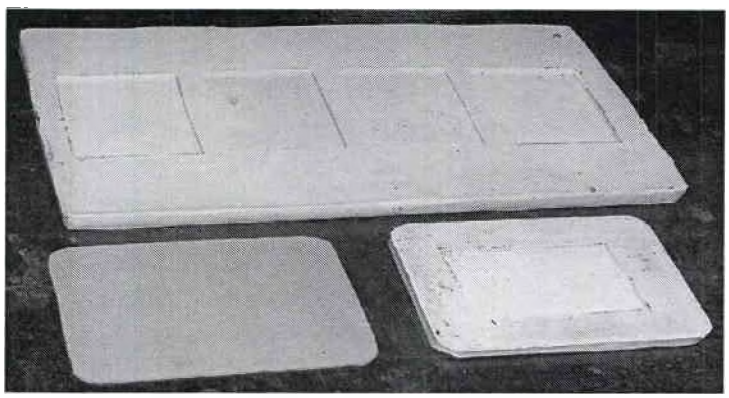

b

c

Fig. 16: Fabrication process of epoxy nanocomposites: a) calendering; b) rubber molds; c) final molded plaque.

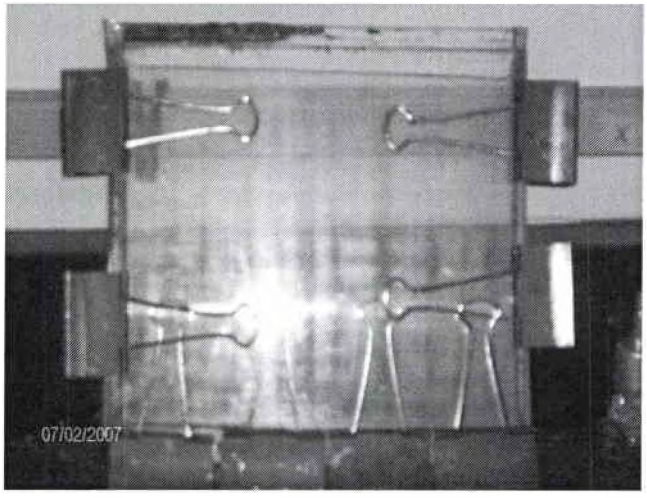

Fig. 17: Glass plate molding system used for epoxy CNT samples.

3.1.3 Fabrication of Advanced Composites

Two additional nanocomposite batches were produced using VGCF batch #94 at 5 wt% and 7.6 wt% in EPON 862/W. This material was formed into approximately 150-micron-thick films using a 3-roll horizontal sheet stack located at UDRI (see Fig. 18). This process involved passing two release films (wax paper type) over and between two heated (60°C), polished, counter-rotating rollers. The resin was placed in a trough between the rollers (Fig. 18a, b), which held the material as it was gradually squeezed out through the bottom in a film of constant thickness. The film sandwiched between the two release plies was then brought over a third roller maintained at room temperature to cool it, and then the film was guided down-stream to a cutting station (Fig. 18c). The resulting film was cut into 15 cm x 15 cm squares and B-staged in an oven at 100°C for about 1 hour. This resulted in a leathery, slightly tacky film (Fig. 18d) with rheology similar to a standard aerospace adhesive film. Total film weight was

approximately 210 g/m^2, with VGCF loading of 10 g/m^2 (5 wt% loading of VGCF) or 15 g/m^2 (7.6 wt% loading of VGCF). A film containing neat EPON 862/W (no VGCF) was also produced.

The resin films were manually interleaved with dry carbon fabric layers using the following lay-up sequence (where "f" indicates a resin film).

[f / 0°/ f / 90°/ f / 0°/ f / 90°/ f / 90°/ f / 0°/ f / 90° / f / 0° / f]

See Figure 19 for photographs. A hand iron was used to help position each resin layer in the fabric before removing the release ply. The lay-ups for all three composites were vacuum bagged and cured in an oven using the recommended cure cycle for EPON 862/W (2 hrs. at 121°C, 2 hrs. at 177°C).

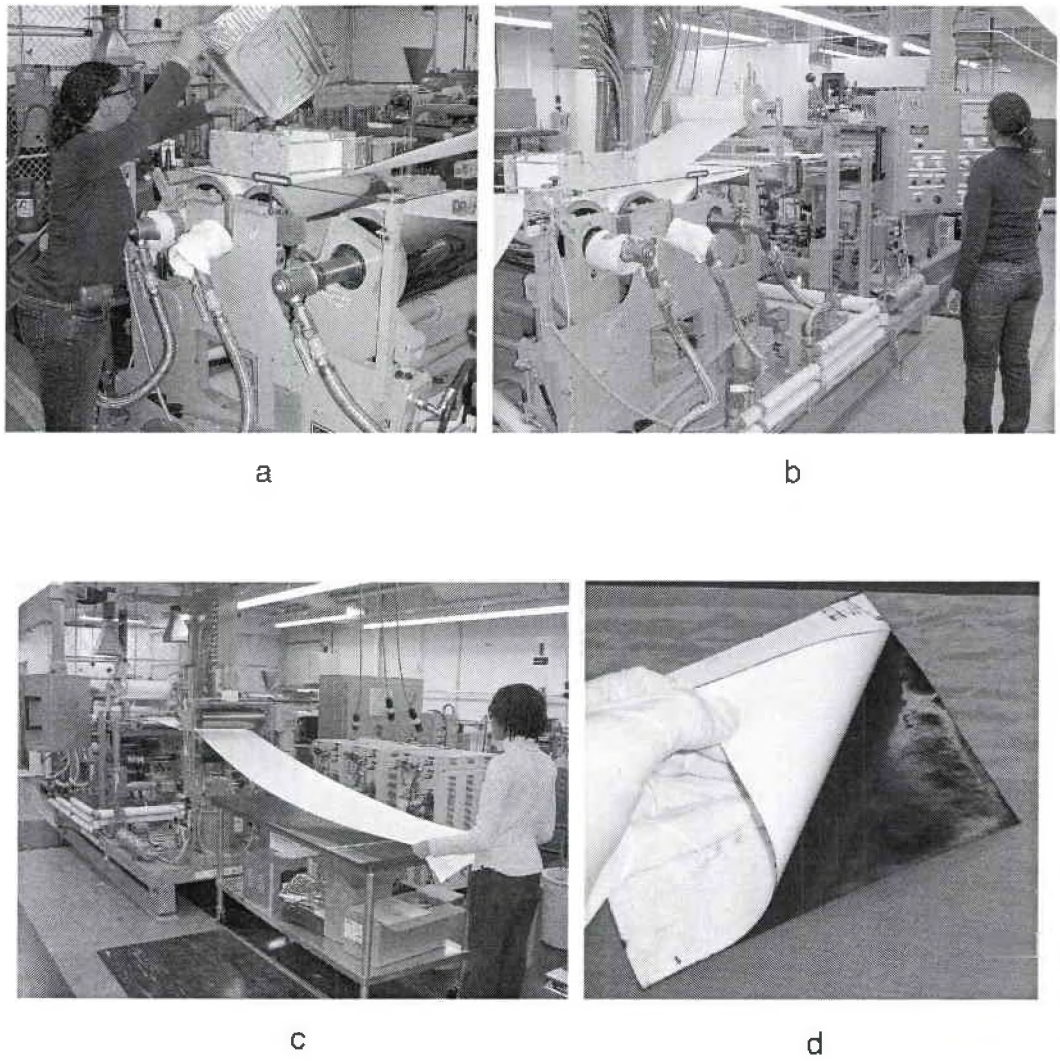

Fig. 18: Film forming process: a) loading the resin trough; b) overall view showing three rollers and release films; c) exit-end of equipment, cutting station; d) peeling back a release ply to show the final film (after B-staging).

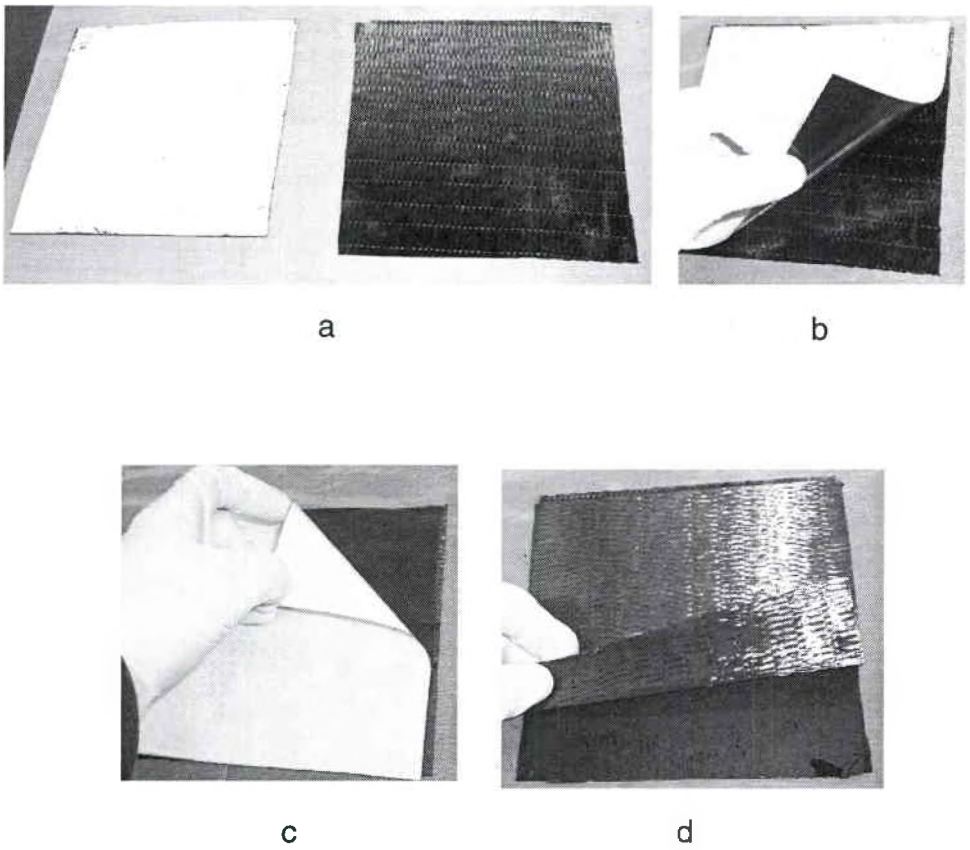

Fig. 19: Composite lay-up, film interleave process. a) Resin film between two white release plies (left) and one layer of dry carbon fabric (right), b) remove bottom release ply and apply to top of carbon fabric, c) remove top release ply from resin film, and d) apply next carbon fabric layer.

3.2 Characterization

The nanocomposites fabricated in this study were analyzed with various methods (e.g. quality analysis, rheology analysis, impact strength test, etc.) to better understand the physical, mechanical, impact and morphological properties. Six techniques were used to describe an overall picture of how nanomaterials affected the properties of the epoxy resin matrix. These modified properties can aid in the decision for composite applications.

3.2.1 Nanofiber/Nanotube Quality Analysis

The first task in this project involved characterizing the incoming raw nanofibers/nanotubes. The bulk density of the as-received dry carbon nanofiber/ nanotube samples was measured as a first step. This procedure involved placing material in a container of known volume and determining the weight. At least two measurements were made for each sample.

For the carbon nanofibers used in this study, residual catalyst level had been previously analyzed by University of Dayton Research Institute via furnace ashing as part of their normal quality control protocol. This involved placing a 1-2 g sample of nanofiber in a ceramic crucible, heating in a furnace to 1000°C in air overnight, and weighing the residue. The residue is comprised fully of oxidized metal catalyst, since carbon oxidizes completely in air around 600°C.

For XD carbon nanotubes, we did not want to expend 1-2 g of material, since our entire stock was 30 g or less. Therefore, Thermogravimetric Analysis (TGA) was used to measure weight loss (20°C/min, air, 3 mg sample).

The morphology of carbon nanofiber materials has been extensively reviewed in other references [26] and so was not included as part of this study. However, the XD carbon nanotube materials were new to this research group, so some time was spent characterizing the morphology via High Resolution SEM. Nanotube samples were deposited on carbon tape and analyzed without sputter coating at 8-10 kV.

3.2.2 Nanotube/fiber Functionalization

The surface oxygen content of nanofiber/tubes was measured with X-ray Photoelectron Spectroscopy (XPS) analysis. Samples were submitted to University of Dayton Research Institute personnel to perform this measurement. A Surface Science Labs SSX-100 XPS spectrometer was used with a base pressure in the analysis chamber of 6×10^{-10} Torr, and an X-ray source with a 600 µm spot size. Samples were prepared by first drying the nanofibers/tubes in a vacuum oven overnight at 100°C or higher, then distributing a small amount of material on copper adhesive tape. Two areas were analyzed on each sample. Results are reported in terms of atom% oxygen in the form of single bonded oxygen (O-C), double bonded oxygen (O=C), and water (H_2O). The signals for single and double bonded oxygen are caused by groups that are covalently bonded to the nanofiber/tube wall, for example in the form or phenolic groups (-OH), aldehyde (-CHO), or carboxylic acid (-COOH).

3.2.3 Nanotube/fiber Gross Dispersion

As a measure of gross dispersion, nanofiber and nanotube dispersion in the matrix was analyzed using microscopy. Uncured resin-nanofiber mixtures were prepared by smearing a thin coat on a glass microscope slide and covering with a cover slip. The goal was to observe the size and concentration of microscopic agglomerates of undispersed nanofibers, which is obvious at magnifications of 50 – 200X. A Nikon microscope fitted with a digital camera was used to acquire images. A graticule with 100 µm divisions was used to calibrate

the field of view for absolute dimensions. All photomicrographs were taken at 50X magnification.

3.2.4 Rheology

The viscosity of the resin system with and without nanotubes and with or without chem-staging was evaluated before and after calendering using a Brookfield Model DV-III Programmable Rheometer. Each sample was tested at 25°C using either spindle 5 or 6 at a speed of 10 – 20 RPM. The testing time was two minutes per sample. Fig. 20 illustrates the rheometer and spindles. Samples were contained in a 110 mL glass container and degassed before measurement. The instrument accuracy was previously verified with fluid calibration standards of 4950 cP and 28,200 cP.

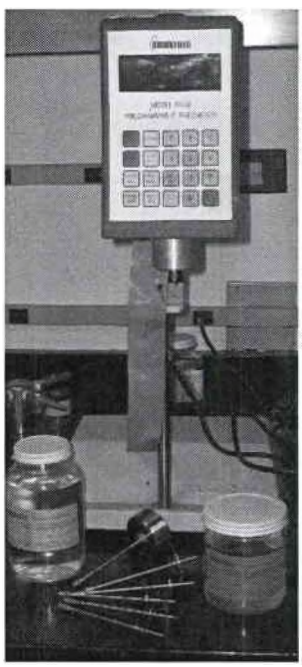

Fig. 20: Brookfield Programmable Rheometer, spindle set, and calibration standards.

3.2.5 Glass Transition Temperature

Cured samples were analyzed for glass transition temperature (T_g) using a TA Instruments Q400 Thermomechanical Analyzer (TMA). Samples were tested in macroscopic expansion mode from 25 to 200°C at a heating rate of 5°C/min in argon. Two specimens were taken from each cured plaque by cutting using a Streus Accutom 5 diamond blade precision wet saw. The typical sample thickness was 3.175 mm (1/8 inch). Each specimen was heated and tested through two heating cycles in the TMA, since the signal from first cycle often contained artifacts from stress relaxation. Fig. 21 shows the TMA device that was used in this study.

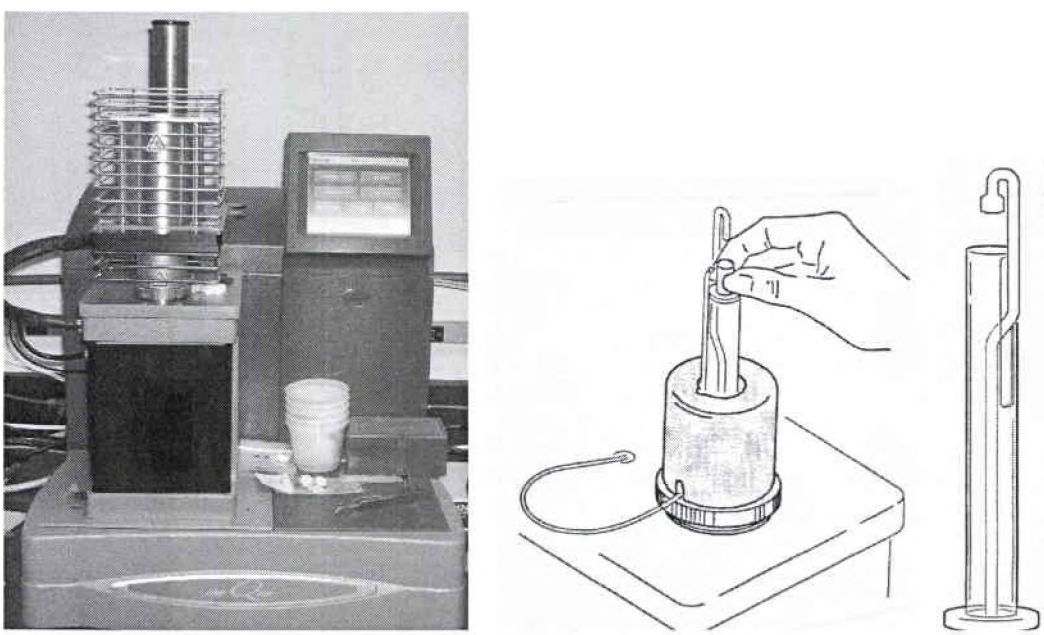

a b c

Fig. 21: a) TMA Q400 system; b) sample stage; c) macroscopic expansion probe (drawn courtesy TA Instruments).

3.2.6 Flexure Properties of Resin Nanocomposites

Nanofiber/resin and nanotube/resin samples were tested according to ASTM D790, "Test Methods for Flexural Properties of Unreinforced and Reinforced Plastics and Electrical Insulating Materials," using an Instron 4486 test machine with a 1000 N load cell, strain rate of 0.127 mm/min (0.05 inch/min.) three point bend fixture, and load span of 5 cm (see Fig. 22). Each cured resin plaque was cut into five 10 cm x 1.25 cm x 0.625 cm bars using a Streus Accutom 5 diamond blade precision wet saw. Once each specimen was placed on the test fixture, an initial contacting force of approximately 9 N (2 lb_f) was applied. Bluehill data acquisition software was used to collect the load vs. extension data. The system was previously calibrated to correct for system compliance. The sample fixture was surrounded with a plastic bag to catch any fragments that became airborne upon failure. Data was exported to a spreadsheet, and modulus was calculated between 0.005 and 0.010 strain units.

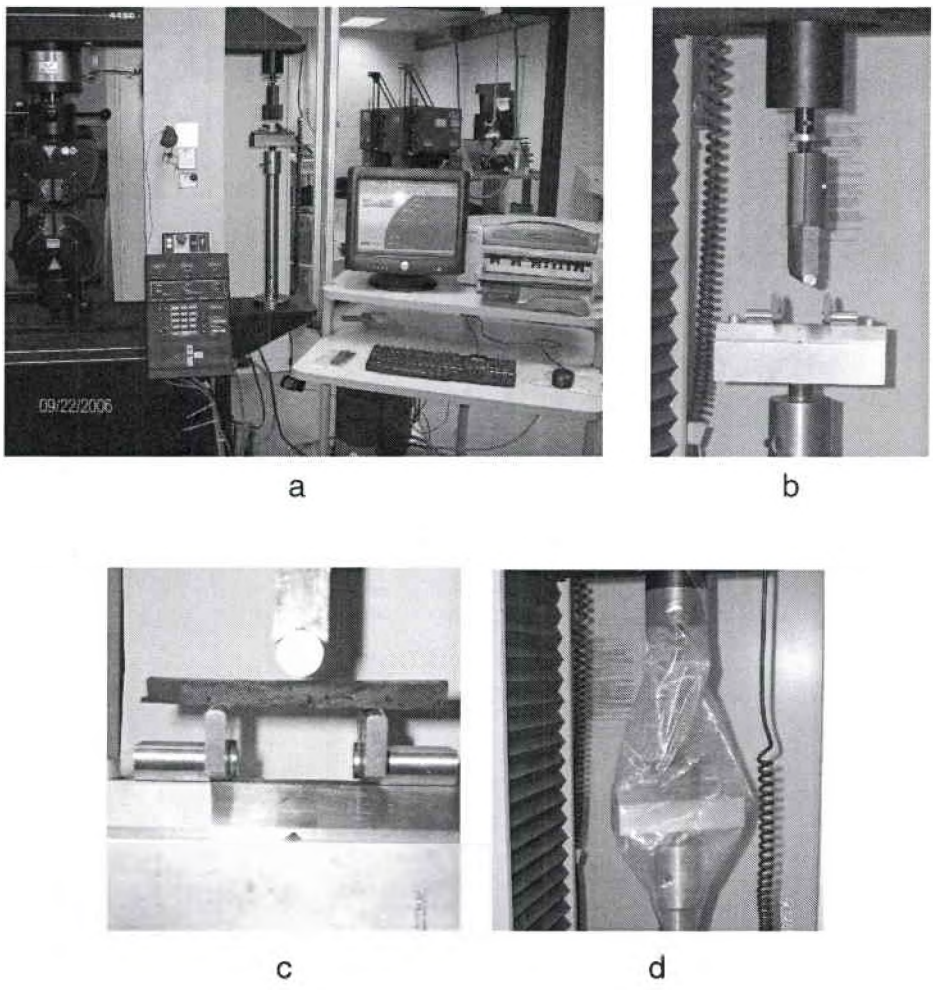

Fig. 22: Flexure testing apparatus: a) load frame and computer system; b) 3-point flex fixture on side frame; c) close-up of loaded specimen; d) specimen wrapped during testing to catch debris.

3.2.7 Impact Properties

Izod impact testing according to ASTM D4812, "Unnotched Cantilever Beam Impact Resistance of Plastics" was performed on the epoxy plaques containing nanofibers and nanotubes, as well as composite laminates containing carbon nanofibers. The Izod Impact apparatus was comprised of a pendulum with striker bar, specimen vise, and dial scale to record pendulum travel (Fig.

23a). Fig. 23b shows the device and testing arrangement for epoxy resin (amber colored) and VGCF-filled resin samples, with an inherent pendulum weight of 454 g (1 lb_m). Specimens 6.35 cm x 1.25 cm x 0.3175 cm were placed in the vise and secured. The pendulum was released to strike the specimen on the narrow side (Fig. 23c). The impact strength was recorded on the dial in the unit of ft-lb_f (where 1 J = 0.7376 ft-lb_f).

The startup procedure for this instrument involved free swinging of the pendulum for 5 minutes. The pendulum was then cocked and swung through one cycle again (with no sample) to record the total travel with no sample resistance. This result was used to determine the wind friction correction factor, which was read from a correction chart. This factor was subtracted from the actual dial reading of the fractured sample to give the corrected impact strength. The results were normalized with the specimen thickness in units of inches (where 1 ft-lb_f/inch = 53.4 J/m).

Composite laminates of similar dimensions were also tested, but their orientation was rotated by 90° along their long axis so that the pendulum impacted the face of the laminate, causing a delamination (Fig. 23d, e). Composite laminates required additional weights to be added to the pendulum such that the total weight was 3632 g (8 lb_m) in order to produce a fracture.

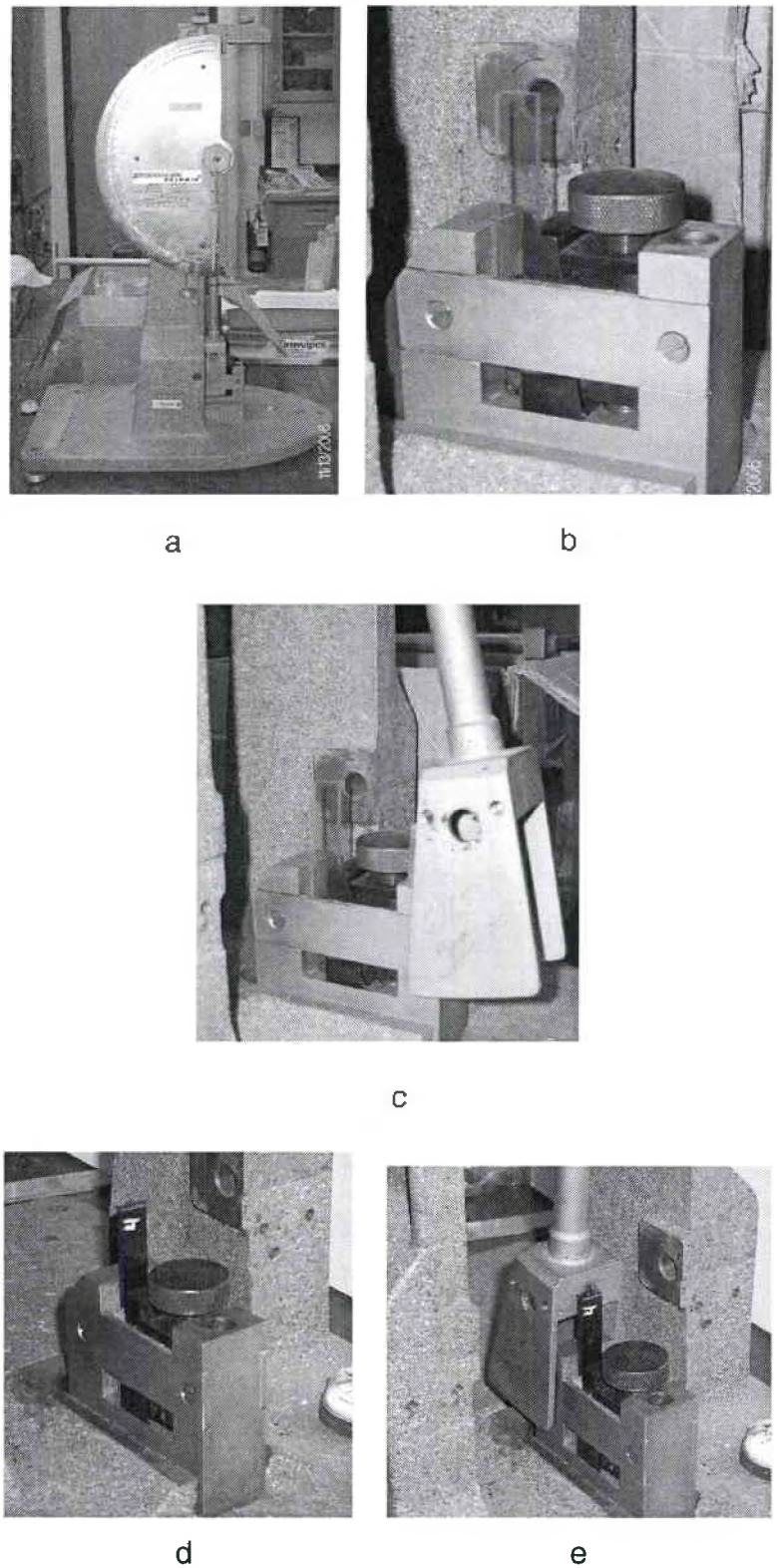

Fig. 23: Izod impact apparatus: a) pendulum at bottom of stroke; b) resin sample in specimen vice; c) resin sample immediately prior to impact from pendulum down stroke; d) orientation of composite laminate sample; e) composite sample after down stroke of pendulum and after snapping back.

3.2.8 Fracture Surface Analysis via Scanning Electron Microscopy

The IZOD impact fracture surfaces of the samples were analyzed using scanning electron microscopy (SEM). Samples were sputter coated with gold for 35 sec at 50 mTorr or platinum/gold for 20 sec at 20 mTorr. A Hitatchi S-4800 High Resolution Scanning Electron Microscope (HRSEM) was used to analyze the coated fracture surface. Fig. 24 illustrates the SEM instrument and sample orientation. Beam energy was 10 or 15 kV and magnification ranged from 200 to 50,000X.

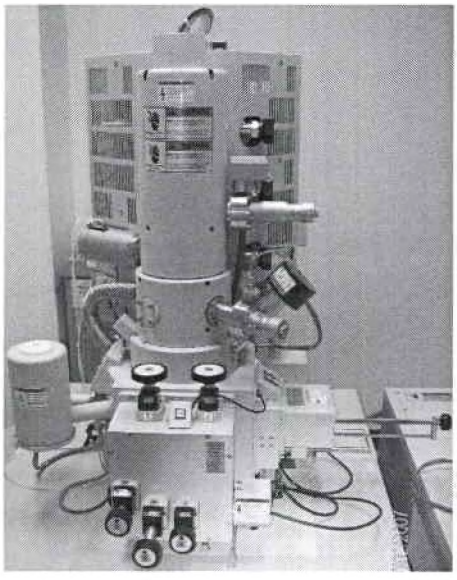

a

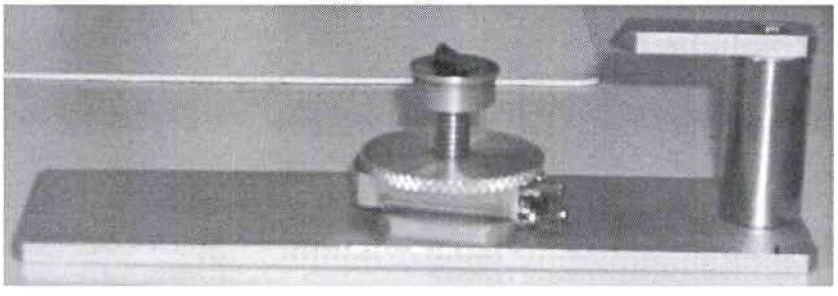

b

Fig. 24: a) SEM apparatus; b) specimen preparation.

CHAPTER 4

RESULTS AND DISCUSSION

4.1 Carbon Nanofiber and Nanotube Characterization

4.1.1 Nanotube/fiber Quality and Morphology

The bulk density of the dry nanofibers/tubes is as follows:

- VGCF batches #71, 104A, and 105B: 0.058 g/cm^3 (3.6 lb/ft^3)
- VGCF batch #94, 106B, and 107B: 0.040 g/cm^3 (2.5 lb/ft^3)
- XD nanotubes as-received: 0.059 g/cm^3 (3.7 lb/ft^3).

Bulk density is indicative of how tightly agglomerated a nanofiber/tube sample is at the micron level. Higher bulk density correlates with tighter agglomeration and increased difficulty of dispersion. However, the presence of residual catalyst will also increase the bulk density, since catalysts used in the nanofiber/tube manufacturing process are typically metallic compounds (usually containing iron).

The residual ash of the nanofiber samples was 1.25 wt%, which implies that the original catalyst was less than 1 wt%. For XD nanotubes, the TGA results (Fig. 25) shows a minimum weight of 8.6% at 660°C. At higher temperatures, the residue (catalyst) gained weight due to oxidation. Thus, the residual catalyst was estimated to be 8.6%, which is higher than that indicated by the certificate of analysis that CNI sent with the XD material (4 wt% residuals).

Since this time, additional information from Rice University has been received indicating methods for removing catalyst and difficult-to-disperse agglomerates. These methods, referred to as "sorting", involve solvent washing and centrifuging. We attempted to implement these techniques (sonicate in acetone or methanol, shear mixing, centrifuge) without success. Specifically, all the material settled to the bottom of the container upon centrifuging. As a result, we abandoned these methods in the interest of moving on with dispersion and sample fabrication. Further study and implementation of these purification methods is recommended. However, the as-received XD material was deemed to be sufficiently pure to continue with the overall study plan, which was originally intended to be an initial effort to gain experience with nanotube materials.

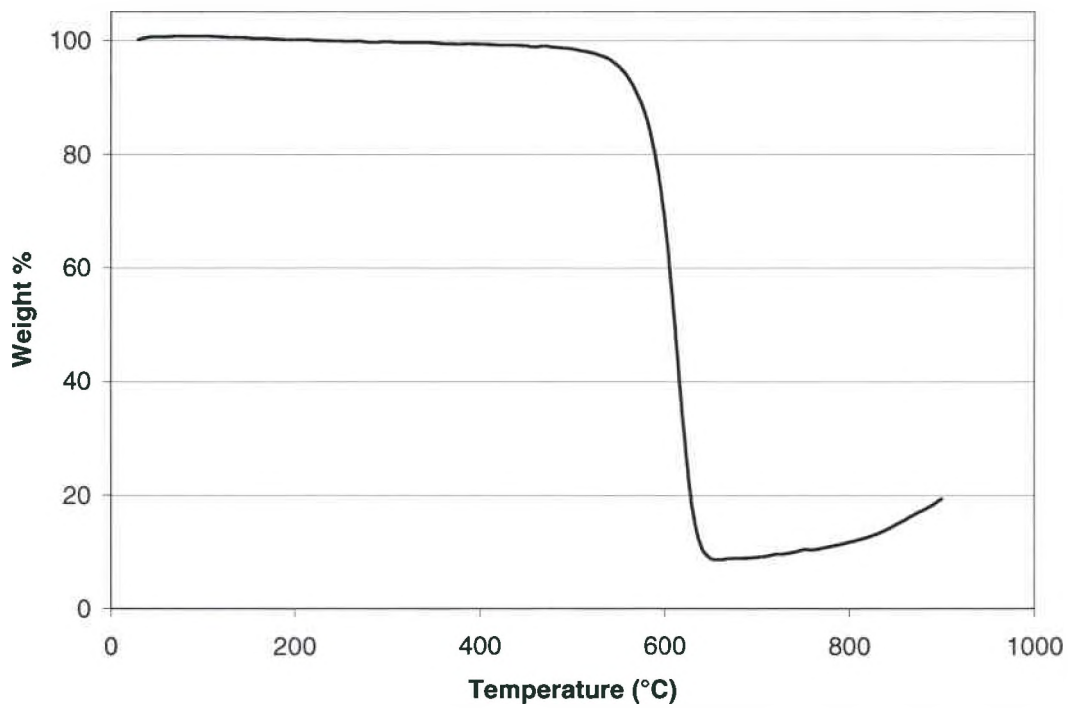

Fig. 25: TGA result for as-received XD nanotubes, 20°C/min, air, 3 mg specimen weight.

The XD material was described by the manufacturer as a combination of single wall, double wall, and higher order carbon nanotubes. The SEM images support this, where a large range of tube diameters were observed, from a few nanometers to 30 nm (see Fig. 26a, b). Some non-tube materials, perhaps catalyst particles, were also observed. At lower magnifications, the tightly nested character of the agglomerates is apparent (Fig. 26c, d). No apparent differences were observed in morphology between as-received and XD, which is consistent with as-received and oxidized nanofiber batches.

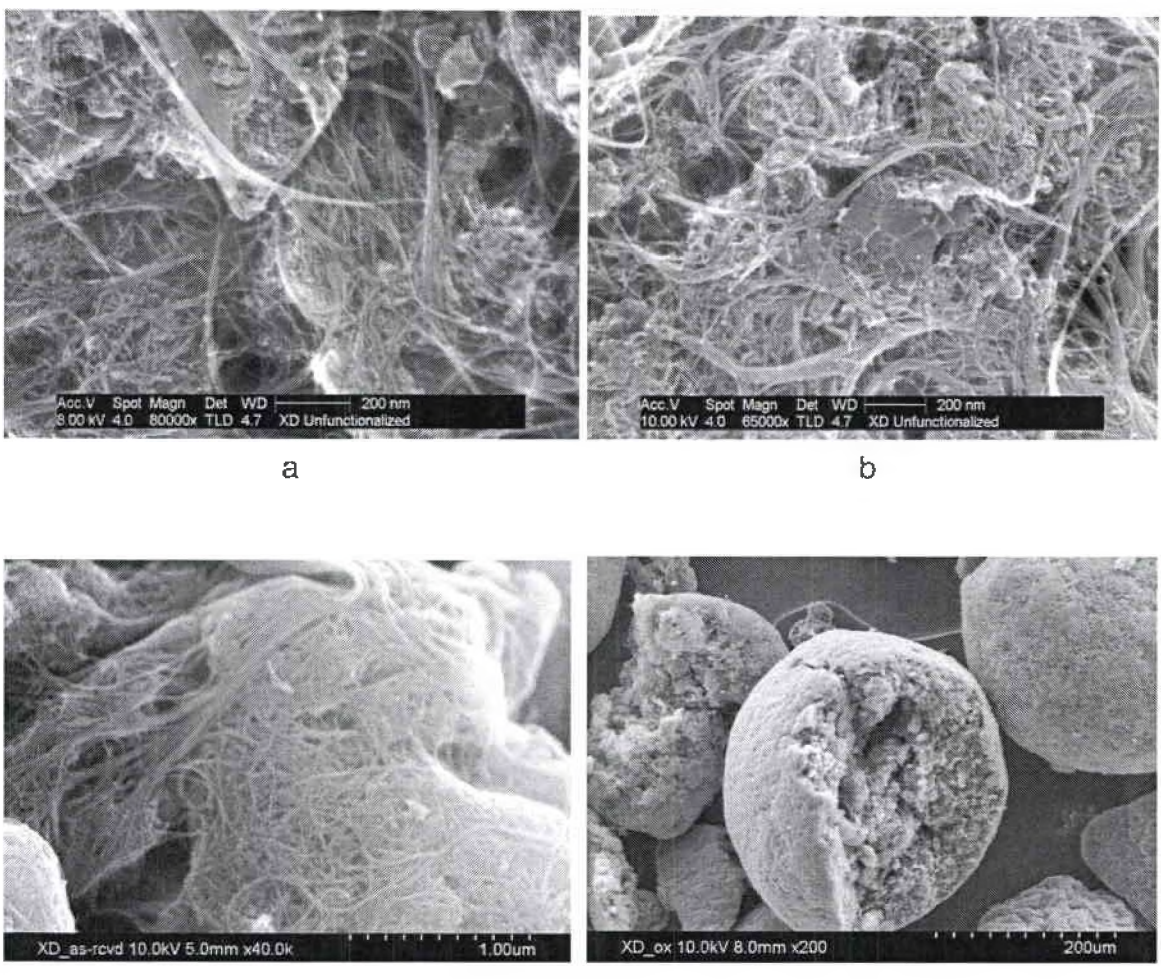

Fig. 26: SEM images of XD carbon nanotube samples, a-c) as-received; d) oxidized.

4.1.2 XPS Results

XPS analysis was used to characterize the degree of functionalization on the nanofiber/tube surface, which in this study was in the form of oxygen. One of the baseline nanofiber samples (batch #71) had a very low amount of oxygen (<1 atom%), as expected because it was unfunctionalized. The oxidized versions of this batch (batches #104A and 105B) exhibited higher oxygen content about 3-4 atom% total. In both cases, the amount of single bonded oxygen was greater than double bonded oxygen, but the ratio changed, especially for batch 105B. The trend in total oxygen was consistent with oxidizing time, where 105B experienced the highest oxidizing time.

Carbon nanofiber batch #94 exhibited a surprisingly high oxygen level, especially for a nonfunctionalized batch. We speculate that this may have been caused during the nanofiber manufacturing process, for example if air had been intentionally or accidentally bled into the reactor. In any case, oxidation of batch #94 led to an *apparent* decrease in oxygen level. We cannot determine with certainty the cause for these results, but we suspect that the margin of error for this measurement is high enough to render the differences in these three batches insignificant. The high level of oxygen in the parent batch (94) may have prevented further addition during oxidation at UDRI.

The as-received carbon nanotube samples had a very low oxygen level, owing to the highly graphitic single and multiwall carbon nanotube surfaces. Oxidation of the XD nanotube (by the same process used for the nanofibers) resulted in a significant increase in surface oxygen: from about 1 atom% total to

over 5 atom%. Interestingly, the ratio of O-C to O=C was opposite that of the nanofiber samples. The amount of surface water was also verified to be negligible, as it was below the detection limits. Table 1 outlines the XPS results for both carbon nanofiber and nanotube materials.

Table 1: XPS results for carbon nanofiber and nanotube raw materials used in this study.

Sample	Oxygen content (atom%)		
	H_2O	O-C	O=C
VGCF #71			
- 1		1.02	< 0.2
- 2		1.33	< 0.2
Average		**1.18**	**< 0.2**
VGCF #104A (#71 oxidized)			
- 1		1.95	1.18
- 2		1.55	1.24
Average		**1.75**	**1.21**
VGCF #105B (#71 oxidized)			
- 1		2.74	1.01
- 2		3.12	1.15
Average		**2.93**	**1.08**
VGCF #94			
- 1		1.08	0.29
- 2		1.09	0.29
Average		**1.09**	**0.29**
VGCF #106B (#94 oxidized)			
- 1		1.53	0.74
- 2		1.92	0.91
Average		**1.73**	**0.83**
VGCF #107B (#94 oxidized)			
- 1		1.89	0.64
- 2		1.94	0.51
Average		**1.92**	**0.58**
XD3365A, As-received			
- 1	bdl[1]	0.56	0.26
- 2	bdl[1]	0.70	0.34
Average		**0.63**	**0.30**
XD3365A, Oxidized			
- 1	bdl[1]	2.27	1.77
- 2	bdl[1]	2.39	1.86
Average		**2.33**	**2.82**

[1] bdl = below detection limits

4.2 Resin-Nanofiber/tube Nanocomposites

4.2.1 Rheology and Molding Technique

The rheology of the epoxy-VGCF samples was not examined in this study, as it has been examined in more detail in previous studies [26]. In all nanofiber batches (#71, 104A, 105B, #94, 106B, 107B), the nanofibers were dispersed into freshly mixed EPON 862/W, which has a viscosity of about 4200 cP. The addition of nanofibers at 8 wt% increased the bulk viscosity to over 100,000 cP, giving the material a paste-like rheology, consistent with previous work at UDRI. Although there may have been slight differences in viscosity depending on nanofiber bulk density and oxygen content, all batches were highly viscous and were not suitable for casting. This is the reason for using a silicone rubber mold and press for curing and consolidating these nanocomposite dispersions.

XD carbon nanotubes, on the other hand, were added to EPON 862/W at a loading of only 0.15 wt%. This had much less impact on the resin bulk viscosity, and thus created new problems. The first concern was considered to be favorable: epoxy-nanotube dispersions were of sufficiently low viscosity to be easily degassed and cast into void-free plaques (potentially), like the neat resin system. However, the low viscosity is counter to the development of high shear stress during the dispersion process. It was found that low resin viscosity also exacerbated the potential for the XD nanotubes to flocculate during the curing process, especially during the initial heat ramp when viscosity dropped to a minimum. For this reason, an approach of increasing the resin viscosity prior to

nanotube dispersion was adopted. The goal was to determine a viscosity that produced a balance of adequate shear stress during dispersion, easy degassing and casting, and low flocculation during curing. Chem-staging was chosen over thermal B-staging because of the more precise control in final viscosity.

The rheology analysis illustrated that chem-staging increased the viscosity of the EPON 862/W in a reasonably even manner (see Table 2). The room temperature viscosity for EPON 862/W, without chem-staging, is 4200 cP. The higher the chem-stage percentage, the more the mixture viscosity increased. Prior to testing each sample, the temperature was checked with an Omega Microprocessor Thermometer, and the Brookfield rheometer was calibrated, to ensure uniform measurements. Table 2 details how the viscosity of the final mixture was affected by curing EPON 862 with a portion Epikure W chem-staging and nanotube dispersion.

Table 2: Matrix viscosity measurements for EPON 862/W chem-staged at different levels, taken at 25°C.

Resin state	Chem-stage level	Spindle no.	RPM	Viscosity (cP)
Immediately after chem-staging (No CNT added)	0%	5	20.0	4,200
	5%	5	10.0	6,000
	10%	6	20.0	15,000
	15%	6	10.0	82,000
After addition and dispersion of XD @ 0.15 wt%	5%	5	15.0	10,500
	10%	5	15.0	22,400
	15%	6	15.0	32,000

The 5% and 10% chem-stage mixtures with addition of CNTs increased in viscosity modestly, while the 15% chem-stage viscosity decreased. This result is unexplained.

The viscosity of the chem-staged epoxy-XD dispersions was sufficiently low to enable casting between two glass plates. This was desired in order to provide plaques with more uniform thickness compared to the rubber molding technique. The neat resin sample (no nano) was easily poured into the mold (both preheated to 60°C) and was cured without voids. The chem-staged/CNT samples were more difficult to pour as a result of higher viscosity, but the mold was able to be filled. However, numerous bubbles were observed, even after degassing the resin at 60°C for 10-20 minutes prior to pouring, which caused voids during curing. An epoxy-XD sample with 0% chem-staging flowed easily, but experienced flocculation during cure. Interestingly, the 0% chem-stage sample containing oxidized XD did not flocculate during curing. However, there were still some voids in the final sample. For this reason, we resorted to the rubber molding technique. In the future, it is recommended that the glass plate technique be tried again, using longer degassing cycles at room temperature so as not to advance the cure any further.

4.2.2 Dispersion Results via Microscopy

Moderate sized agglomerates (20-50 μm in diameter) were apparent in the uncured resin when viewed at 50X magnification. A representative image from each batch is given in Fig. 27. Additional passes beyond four in the dispersion

process did not lead to any apparent improvement in the results. Dispersion quality varied among the nanofiber batches, possibly related to the level of surface oxidation, where increased surface oxidation led to higher dispersion uniformity. However, dispersion quality was also believed to be related to the degree of initial agglomeration in the raw material, which varied somewhat among the batches. Batch #94 was better dispersed than #71, as predicted by the bulk density results. Oxidation generally improved the dispersion quality, although there was no specific correlation with XPS results.

The XD-epoxy dispersions also contained agglomerates of approximately the same size distribution as the nanofiber samples (see Figure 28). It was difficult to discern any difference between the chem-stage levels with confidence, but we may have detected a decrease in the number of small agglomerates with increasing chem-staging although large agglomerates are still present (Figure 28 a-c). The oxidized XD nanotubes appear to have even fewer small agglomerates, although again the large agglomerates are still present. It may not be possible to disperse these larger agglomerates with the current process, and therefore it is recommended that future research be conducted towards implementing "sorting" techniques to help condition the raw material prior to dispersion. Also, further studies should employ quantitative particle size distribution analysis techniques that are coming on-line. This would provide a non-subjective measure of dispersion quality.

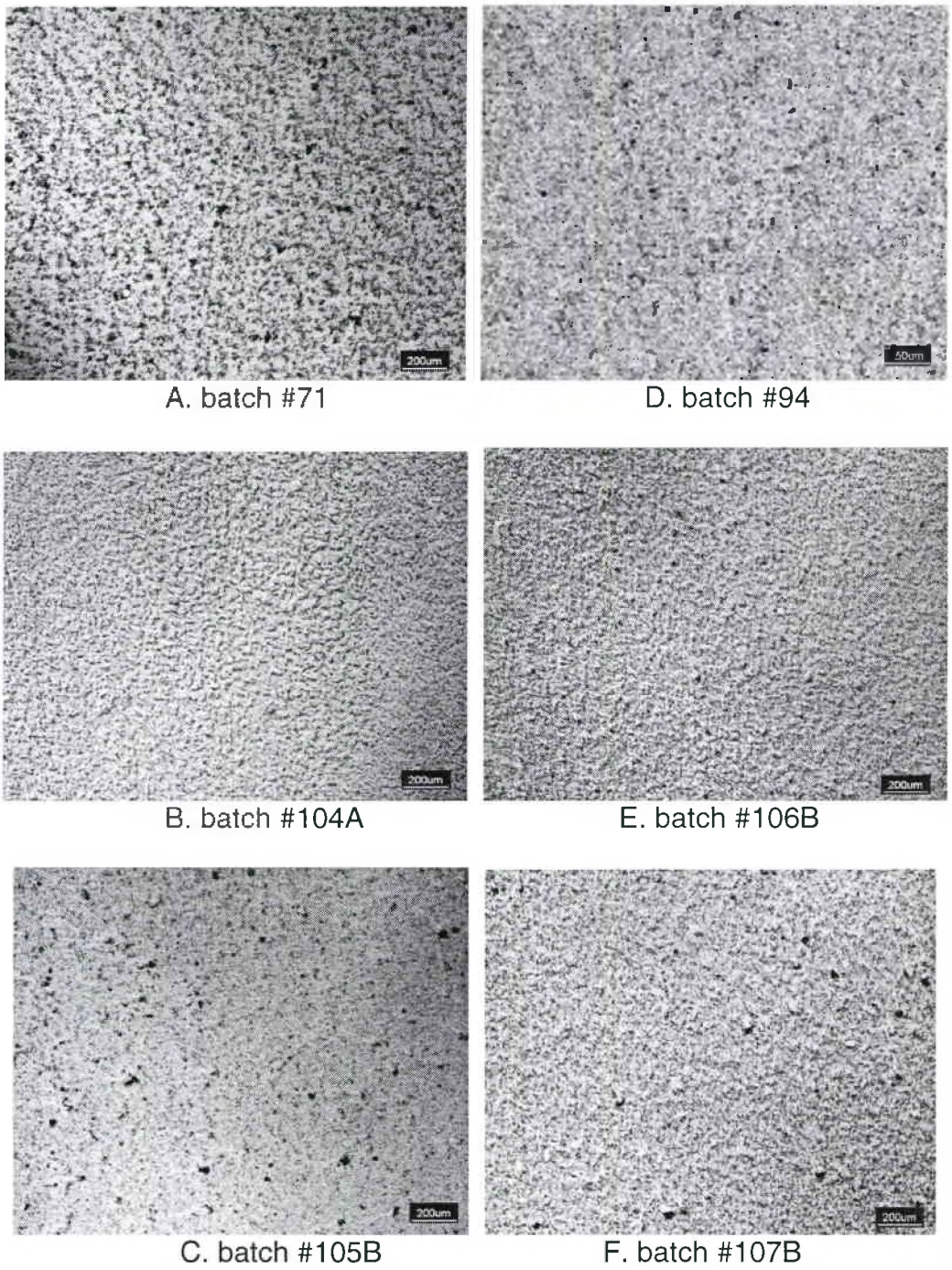

Fig. 27: Photomicrographs of VGCF @ 8 wt% in EPON 862/W after calendaring (50X magnification): A) batch #71; B) batch #104A; C) batch #105B; D) batch #94; E) batch #106B; F) batch #107B. Black spots are the remaining agglomerated nanofibers.

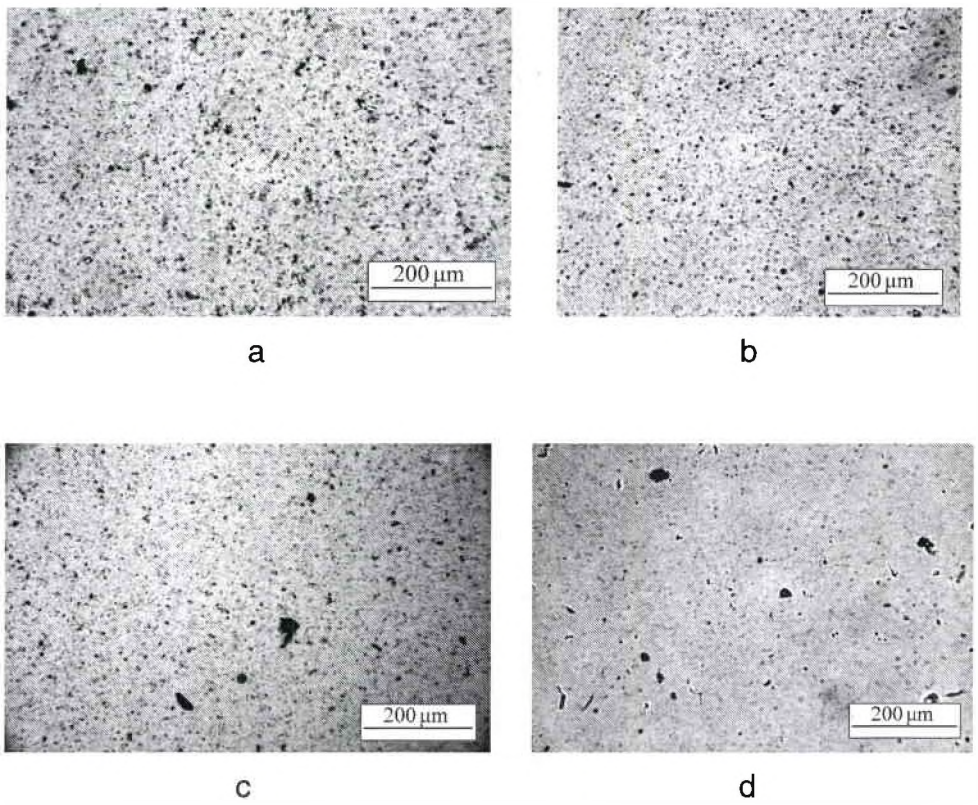

Fig. 28: Dispersion results for XD carbon nanotubes: a-c) 5%, 10% 15% chem-staged in EPON 862/W with as-received XD at 0.15 wt%, and oxidized nanotubes in EPON 862/W (0% chem-stage) at 0.15 wt%.

4.2.3 Glass Transition Temperature and Flexure Strength

The plaques containing carbon nanofibers were analyzed for both T_g and flexure strength (Table 3). The T_g values were essentially the same or slightly higher than the neat resin, indicating that epoxy network formation was not affected negatively by the presence of functionalized nanofibers. The unfunctionalized nanofiber degraded flexure strength compared to neat resin, but two of the functionalized nanofiber batches demonstrated a significantly higher

modulus with similar or improved strength (VGCF batches 106B, 107B). Further study is needed to explain why certain functionalized nanofiber batches outperformed the others. No trend in properties with surface oxidation level was detected. Perhaps more specific information is needed about which types of oxidized chemical groups (hydroxyl, carboxylic acid, carbonyl, anhydride, etc.) are required before a deeper understanding can be established.

Table 3: Glass transition temperature and flexure results for VCGF-epoxy samples.

VGCF batch #	Nanofiber XPS results	TMA results[1] *(σ shown in parentheses)*	Flexure Test Results [2] *(σshown in parentheses)*		
	surface oxygen (atom%) O-C O=C	T_g (°C)	Modulus (GPa)	Strength (MPa)	Strain to failure (%)
None (neat 862/W)	N/A	147 (6.7)	3.34 (0.16)	143 (2.9)	7.0 (2.5)
#71	0.55 0.40	154 (2.3)	3.85 (0.45)	109 (2.4)	4.1 (1.0)
#104A (#71, oxidized)	1.75 1.11	149 (3.4)	2.51 (0.12)	97 (3.5)	5.8 (1.6)
#105B (#71, oxidized)	2.93 1.08	152 (2.1)	2.96 (0.91)	99 (3.3)	5.7 (0.7)
#94	2.30 0.55	146 (3.1)	3.00 (0.09)	118 (0.9)	5.7 (0.3)
#106B (#94, oxidized)	1.73 0.83	153 (1.9)	7.94 (0.32)	184 (3.0)	4.9 (1.5)
#107B (#94, oxidized)	1.92 0.58	149 (8.7)	5.29 (0.12)	133 (1.9)	3.5 (0.6)

[1] four specimens per cured panel (2 locations, heat and reheat each location)
[2] five specimens per cured panel

4.2.4 Impact Strength

Izod impact results for carbon nanofibers, given in Table 4, show a fairly large variability within each plaque (typical 25% coefficient of variation). This variability may be partly due to the sample to sample variation in specimen thickness caused by the rubber molding technique. However, two separate plaques made of the same batch of resin exhibited very similar average results. It is suspected that the overall variability would narrow if notched specimens would be used (ASTM D256), although this would require more time and effort for sample preparation. The results for the nanofiber-reinforced resin samples were generally lower than that measured for neat resin. However, VGCF Batch #106B exhibited an increased impact strength compared to neat resin. This is interesting since VGCF batch #106B had the highest flexure strength (Table 3).

Table 4: Izod impact results for VGCF-epoxy samples (5 specimens per plaque)

VGCF batch #	Impact Strength, J/m (C.O.V.)[1]	
	plaque #1	plaque #2
None (neat 862/W)	486 (18%)	N/A
#71	406 (28%)	368 (25%)
#104A (#71, oxidized)	438 (43%)	470 (22%)
#105B (#71, oxidized)	342 (87%)	N/A
#94	443 (22%)	N/A
#106B (#94, oxidized)	603 (7%)	N/A
#107B (#94, oxidized)	401 (26%)	454 (23%)

[1]Coefficient of variation (C.O.V) = standard deviation / average

Table 5 illustrates that the carbon nanotubes Izod impact results also show a sizeable variation. The impact strength was higher in the nanotube reinforced specimens compared to the neat resin indicating that even at a low weight percent, 0.15 wt%, the impact strength can be increased significantly. The test also showed that chem-stage processing led to more uniform dispersion and therefore produced more consistent properties. Overall, the chem-stage samples trended toward higher resistance than neat resin. However, because of high coefficient of variation, these improvements are not statistically significant. The molding process, as well as the dispersion process, must be improved to provide uniform sample thickness.

Table 5: Izod impact data for XD nanotube-epoxy samples (5 specimens per plaque)

CNT batch #	Impact Strength, J/m (C.O.V.)	
	plaque #1	plaque #2
None (neat 862/W)	486 (18%)	N/A
0% Chem-stage	540 (42%)	469 (43%)
5% Chem-stage	524 (24%)	494 (30%)
15% Chem-stage	478 (24%)	502 (37%)

4.2.5 Fracture Surface – SEM

Figure 29 shows the fracture surface after impact of sample #106B. At 30X magnification, one can observe the surface has various elevations and that the specimen was extremely rigid as is indicating the fracture "river" patterns, which appeared coarse (Figure 29a). At 2000X, the distribution of the carbon nanofibers is detected. The nanofibers in this specimen appear evenly dispersed; a typical example is given in Figure 29b. This feature could contribute to the sample's high impact strength. Magnifications of 10,000X and 50,000X (Fig. 29c and d) illustrate the nanofibers pulled from the resin. The holes represent the area where carbon nanofibers were located before impact. A few nanofibers can be seen to be broken off, which indicates the tight bond with the resin matrix. The other samples had similar morphology, so it was impossible to make a conclusion as to why sample #106B exhibited higher impact and flexure strength. None of the samples had obvious agglomerates on the fracture surface.

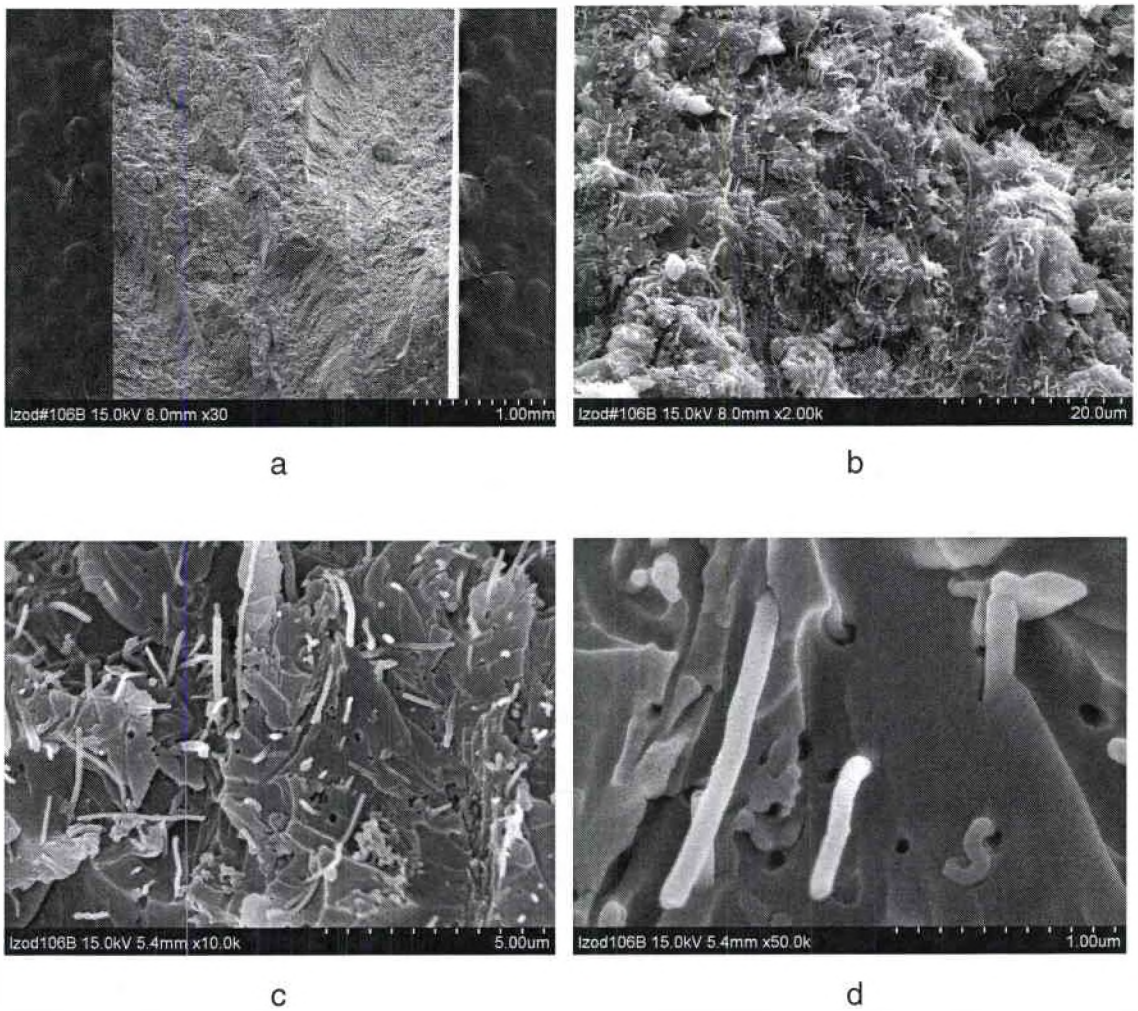

Figure 29*:* Impact fracture surface of epoxy resin sample containing 8 wt% VGCF #106B: a) 30X; b) 2000X; c) 10,000X; d) 50,000X.

The Izod impact fracture surface for neat resin is given in Figure 30. Although there are some features, the surface is generally smooth. All the XD nanotube samples exhibited a more featured fracture surface. A common feature covering part of the surface resembles "hills and valleys" (Figure 31 a-b). Upon closer examination the hills and valleys were usually associated with the presence of fibers of approximate diameter 1-5 μm. Furthermore, the fibers were largely aligned in the direction of the valleys. The size range of the fiber-like

particles is too large for a nanotube, but too small for a human hair. This result was puzzling and not obtained previously with neat resin or nanofiber samples. The orientation of the fibers may have contributed to good quality bonding at the interface. At higher magnification the MWNTs can be seen (Fig. 31 e-f). Nanotube distribution was light and did not appear to be uniform, and agglomerates were observed. This heterogeneity explains the large variation in impact strength data. Additional work is needed to improve dispersion, and additional study is needed to determine the nature of the large fibers present.

An example of an excessively large fiber is given in Figure 30 g-h. It is not certain whether this is a contamination (e.g. a hair) or an extremely large example of the micron-sized fibers described above.

A complete set of fracture surface SEM images are located in the Appendices for neat resin, 0%, 5%, and 15% chem-stage.

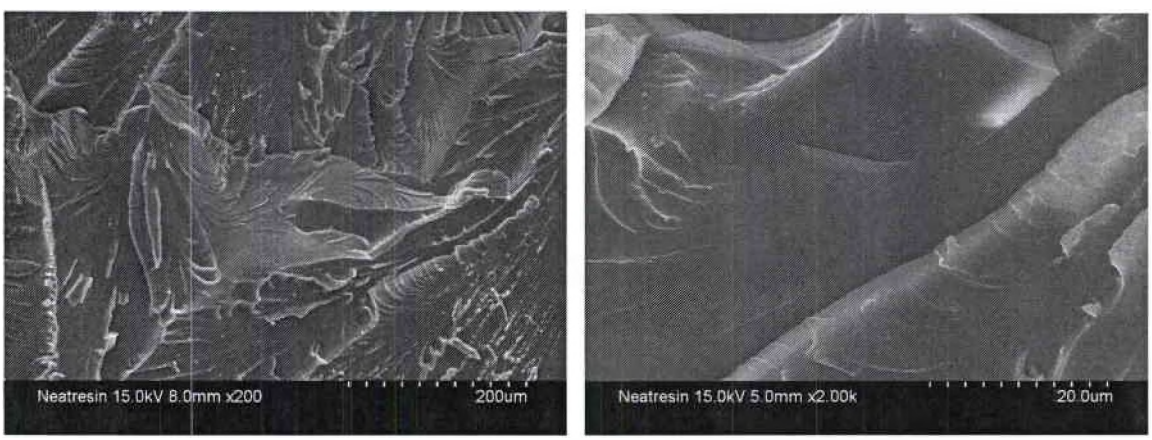

a b

Fig. 30: Izod impact fracture surface of neat resin samples.

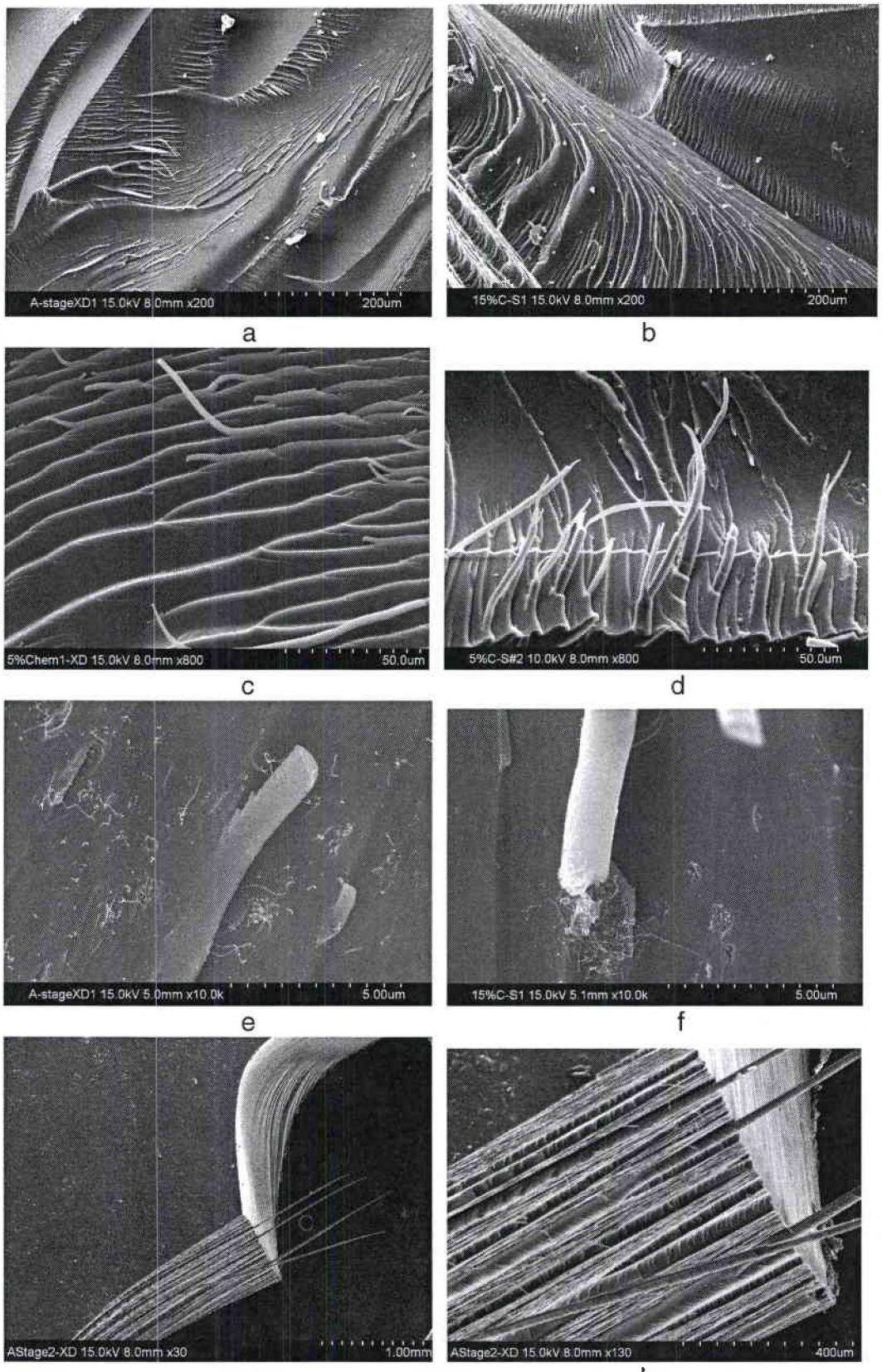

Fig. 31: Izod impact fracture surface of epoxy-XD samples.

4.3 Composite Laminate Characterization

4.3.1 Microscopy, Fiber Volume Fraction

The cured composite laminates were cut, polished, and examined with microscopy (Figure 32). The results indicated some intralaminar dryness and interlaminare resin-rich conditions. The fiber volume fracture of the laminates was estimated to range from 41-45% based on thickness measurements, fiber theoretical density, and carbon fabric weight. These problems can be resolved in the future by adjusting the cure cycle and/or using an autoclave to apply higher pressure during cure. However, the panels were of sufficient quality to test. These panels are referred to as "nano-fiber reinforced composite laminates."

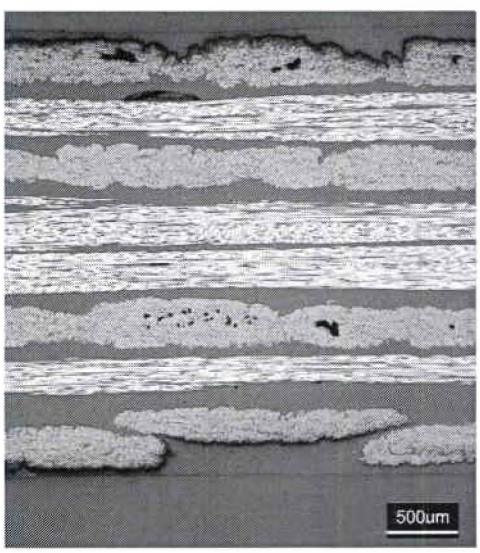

Figure 32: Photomicrograph of cured nano-fiber reinforced composite laminate.

4.3.2 Impact Strength

The laminated composite samples were tested only for Izod impact strength. The load on the pendulum was increased from 1 pound to 8 pounds in order to allow the pendulum to swing through the laminates, causing delamination, fracture of 90° plies, and even tensile fracture of some of the 0° plies. The specimens snapped back into position in some cases. The composite values given in Table 6, are about the same as those of the neat resin. This is because the apparatus is calibrated for specimens with a linear distance of 1.25 cm parallel to the pendulum swing direction, and a pendulum weight of 8 lbs. Because of these differences in the way the neat resin specimens were tested, the results for the composite laminates therefore represent relative values. The laminates containing carbon nanofibers exhibited significantly greater impact resistance than the laminate without nanofibers.

Table 6: Izod impact data for Nanofiber-Reinforced composite laminates.

Nanoparticle (loading)	Impact Strength, ft-lbs/inch (C.O.V.)
No nanofiber (carbon fiber / epoxy only)	5.2 (12.7%)
VGCF #94 (10g/m^2/ply)	9.0 (8.8%)
VGCF #94 (15g/m^2/ply)	9.1 (8.5%)

4.3.3 Fracture Surface – SEM

SEM images of the composite fracture surface are given in Fig. 33. At 30X magnification (Figure 33a) the fracture surface is observed to be covered mostly with resin, although some bare carbon fibers are visible. The direction of the carbon fibers in the top ply is clearly aligned from top to bottom in this image. Magnification of 2000X (Figure 33b) illustrates the nanofibers surrounding carbon fiber. In other images (not shown here), empty troughs could be seen where the carbon fiber had once been located. Closer analysis shows pull-out of individual nanofibers from the matrix (Figure 33c). These images indicate good dispersion of the carbon nanofibers between each ply of the laminate and close contact between the nanofibers and the carbon fabric (Figure 33d). Toughening the area in between plies is crucial to improving overall composite toughness because it usually is the weak link where cracks can propagate.

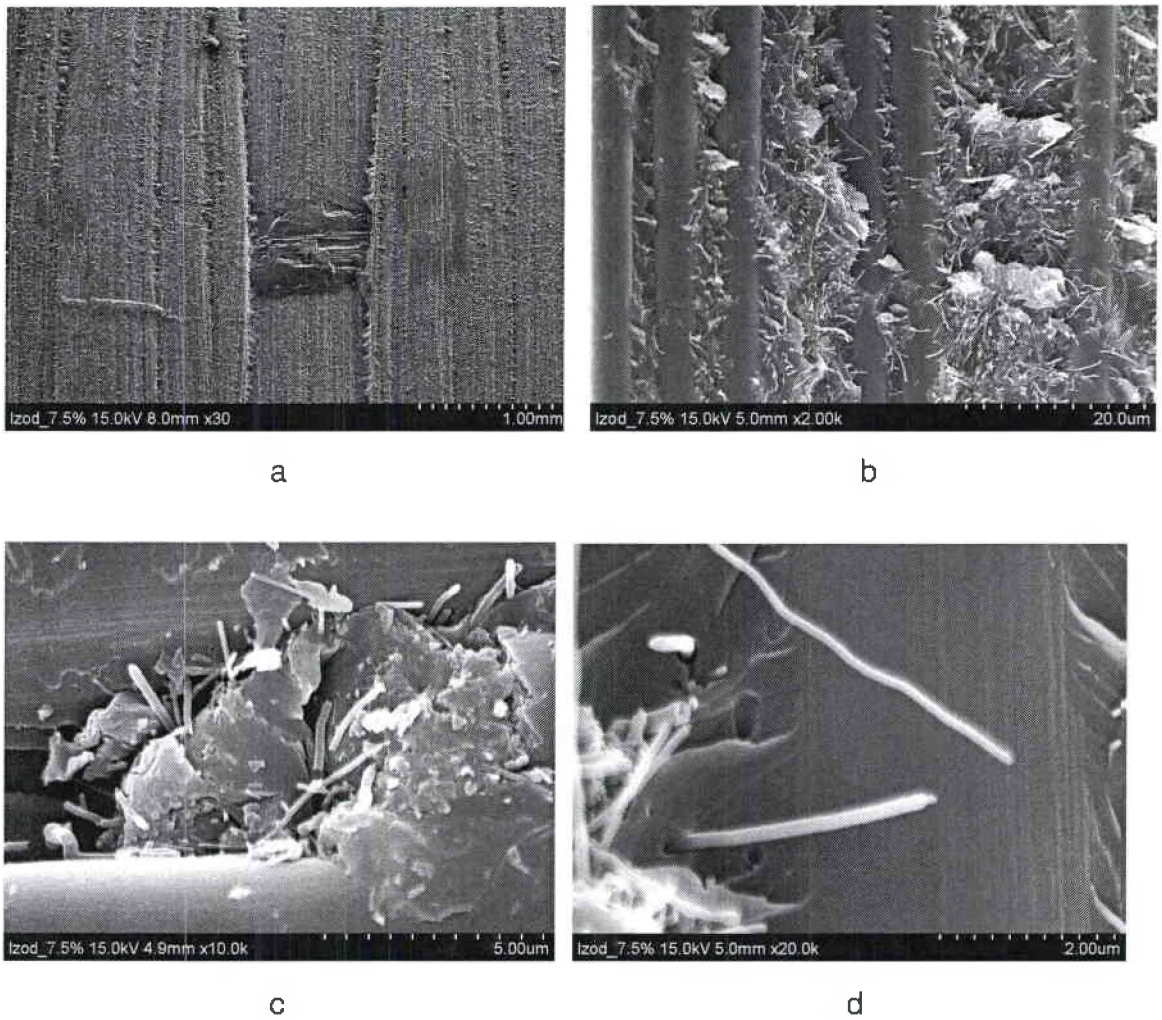

Figure 33: Izod impact fracture surface of composite laminate containing 15 g/m^2/ply, VGCF #94 at a) 30X; b) 2000X; c) 10,000X; d) 20,000X.

CHAPTER 5

CONCLUSIONS AND RECOMMENDATIONS

The research performed during this program demonstrated straightforward and scaleable methods for fabricating, analyzing, and testing polymer nanocomposites, as well as continuous fiber laminates containing a nano-modified matrix. The results from this research varied with the nanomaterial, nanomaterial loading, and processing steps. Overall, the work served to identify issues in each area that need to be addressed before further progress can be made in fabricating high quality nanocomposite materials. The most critical of these is obtaining uniform nanotube distribution, and removal of difficult to disperse agglomerates.

5.1 Carbon Nanofibers

The major accomplishment was demonstrating a simple and scaleable process to produce a modest, although not perfect, dispersion of carbon nanofibers. Although most of the nanofibers were de-nested, a number of agglomerated nanofibers about 10-50 micrometers in diameter remained. The batches containing oxidized nanofibers appeared to have fewer and smaller undispersed agglomerates than those with non-oxidized nanofibers. The oxidized nanofibers

improved the T_g of the epoxy resin by 0-7°C, indicating that the epoxy network formation was not negatively affected by the presence of the functional groups on the nanofibers. The flexure strength and Izod impact strength was generally degraded by the nanofibers, but one batch of oxidized nanofibers exhibited a significant improvement in each. Additional study is required to repeat these results and determine what it was about that batch that created the improved results. The level of oxygen detected by XPS did not correlate with any of the results. In any case, the sample molding quality needs to be improved before further progress can be demonstrated. Also, newer grades of Pyrograf III are available on an experimental basis (PR-25) that are generally easier to disperse which should be examined in future studies.

5.2 Carbon Nanotubes

The major accomplishment was producing acceptable nanotube epoxy composites for initial property screening. The epoxy-XD nanotube dispersions were not homogeneous. This was especially apparent due to the low loading. A process for conditioning the raw material and "sorting" nanotubes must be implemented before further progress can be made. Oxidizing the XD nanotubes increased their compatibility with the matrix, enhanced dispersion, and minimized flocculation. Nanotube-reinforced matrix impact strengths were higher compared to the non-reinforced epoxy matrix for all chem-stage levels. Because the nanotubes were not functionalized, the interfacial bonding between the matrix and nanotubes was not optimized. Therefore, further research using

functionalized nanotubes should be conducted. Additional work is needed to optimize the chem-staging process and degas cycle so that the glass plate molding technique can be used, in order to provide uniform thickness samples.

5.3 Carbon Fiber Laminates

The major accomplishment was demonstrating that out-of-plane mechanical properties of composite laminates can be improved with incorporation of a nano-modified matrix. Impact results were significantly improved with the use of a nanofiber-reinforced matrix compared to composites with only an epoxy matrix. However, these composites represent an initial trial, and the quality was not optimized. Factors such as void content and fiber volume fraction may have influenced the results. Some additional development is required to optimize the cure cycle for the nano-modified composites, taking into account the increase in bulk resin viscosity and B-staged state of the resin films. In addition, other issues such as debulk cycle and use of an autoclave should be considered.

APPENDIX A

NEAT RESIN FRACTURE SURFACES – SEM

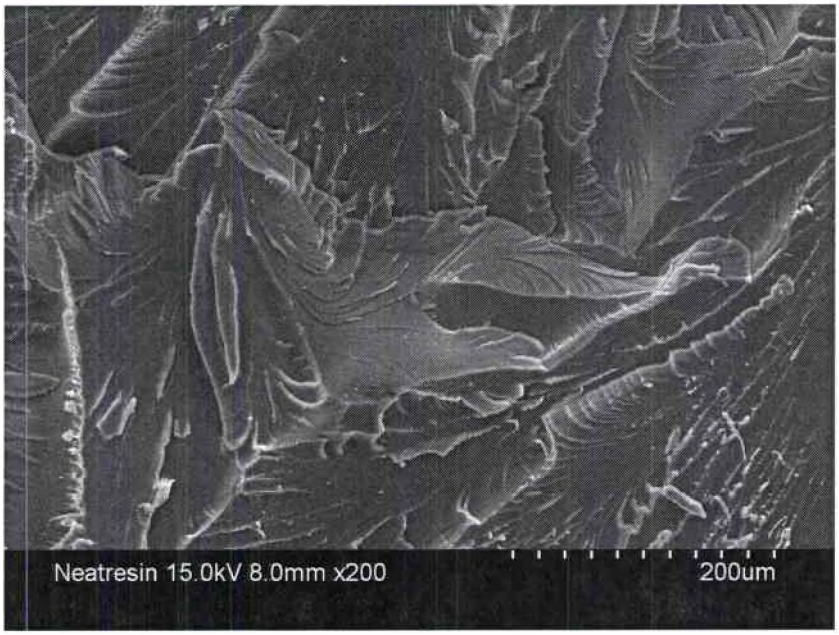

Fig. A.1: Neat resin fracture surface at 200X magnification.

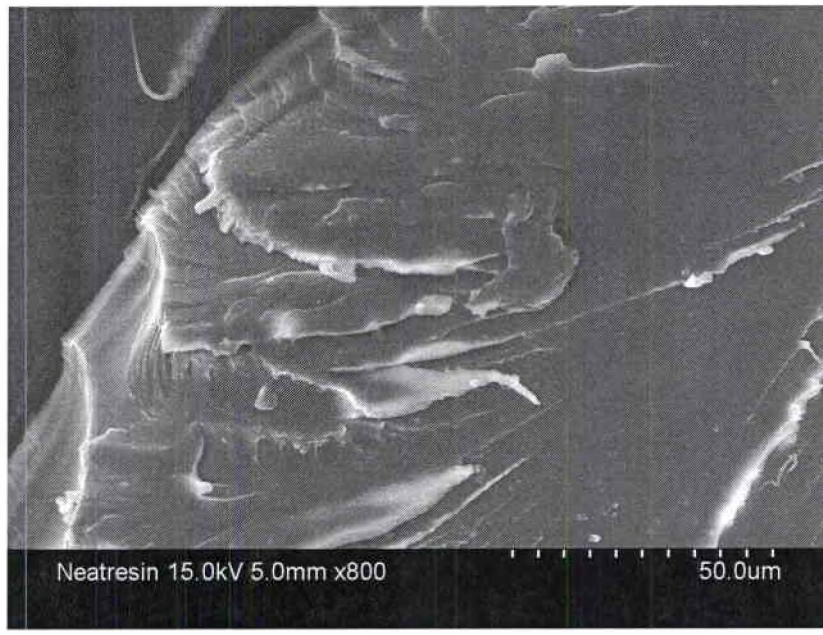

Fig. A.2: Neat resin fracture surface at 800X magnification.

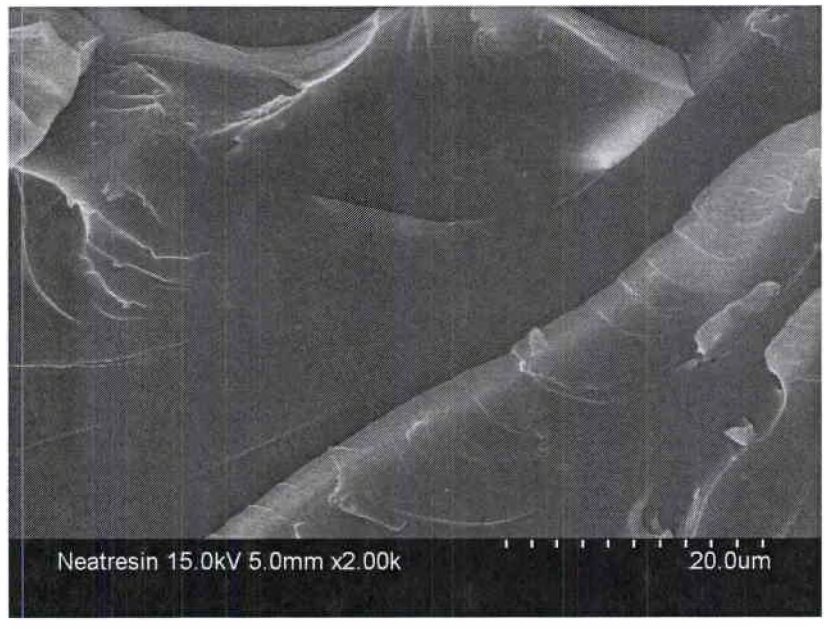

Fig. A.3: Neat resin fracture surface at 2000X magnification.

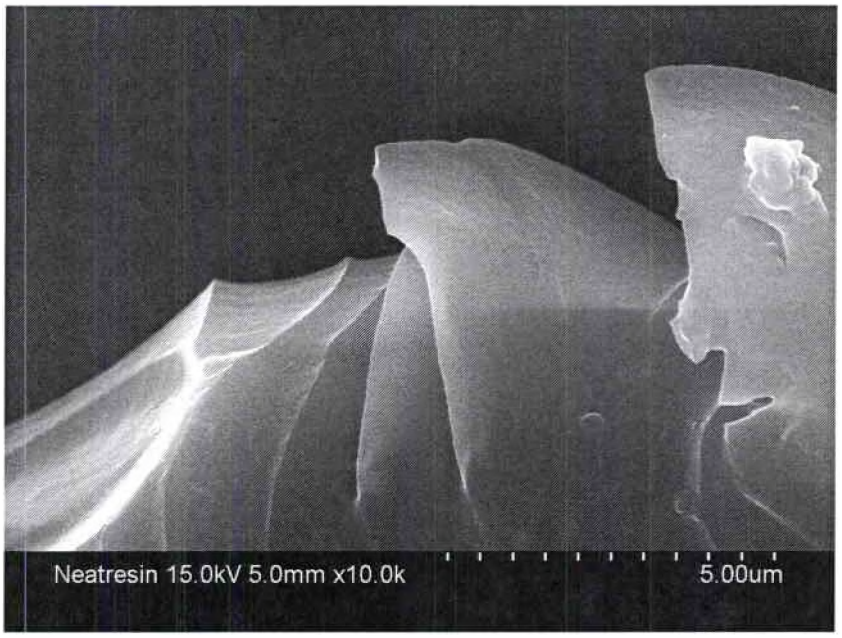

Fig. A.4: Neat resin fracture surface at 10,000X magnification.

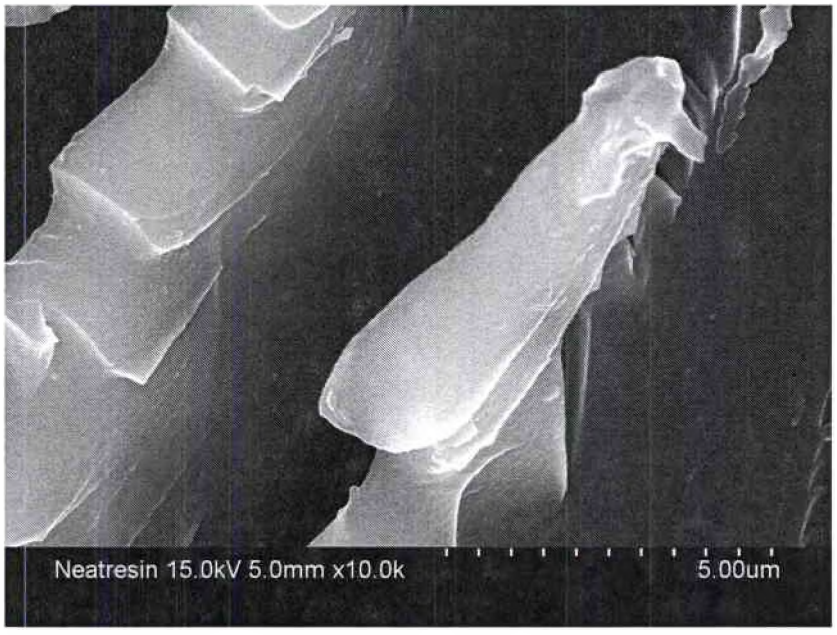

Fig. A.5: Neat resin fracture surface at 10,000X magnification.

APPENDIX B

0% CHEM-STAGE FRACTURE SURFACES – SEM

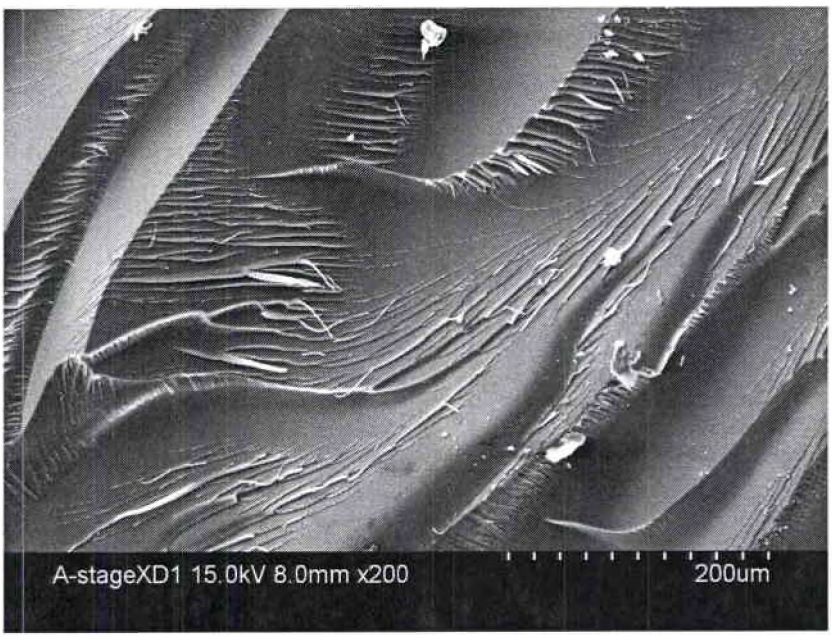

Fig. B.1: 0% Chem-stage fracture surface at 200X magnification.

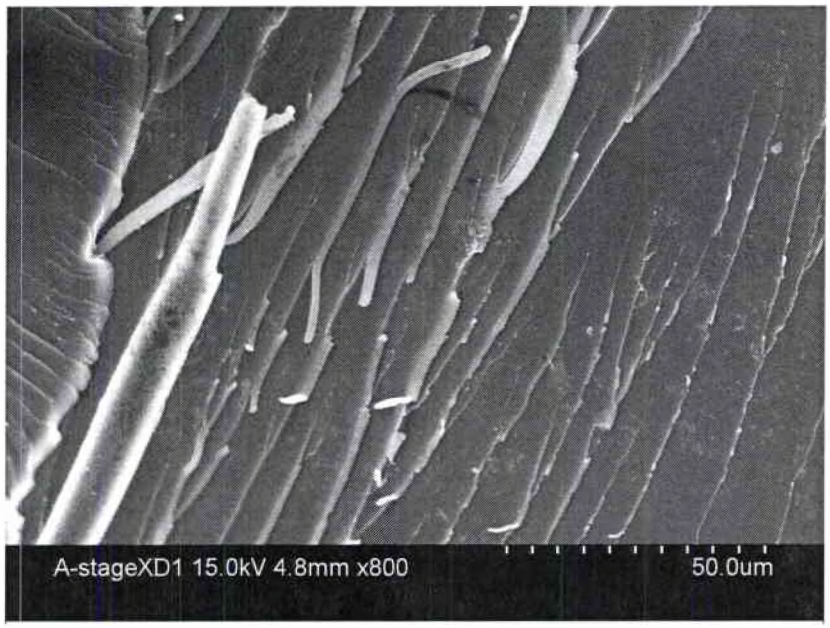

Fig. B.2: 0% Chem-stage fracture surface at 800X magnification.

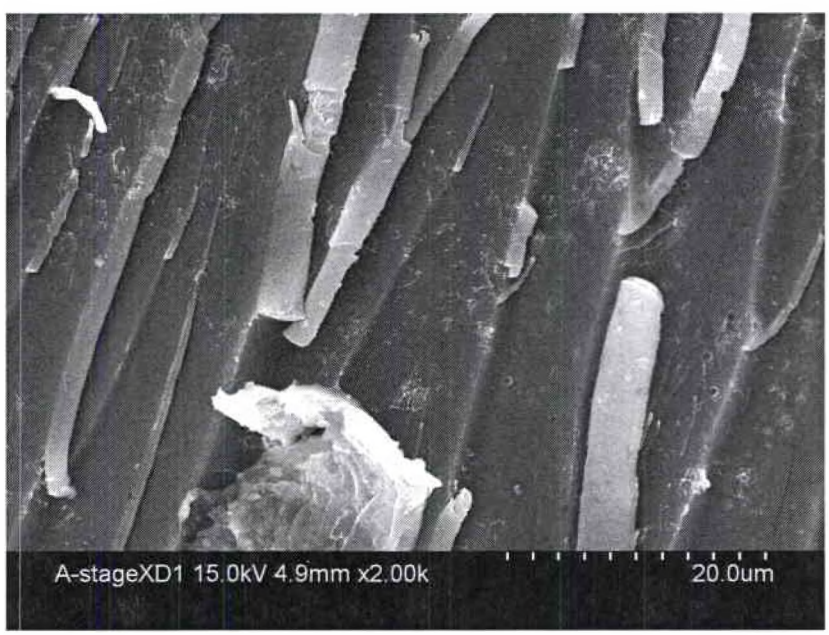

Fig. B.3: 0% Chem-stage fracture surface at 2000X magnification.

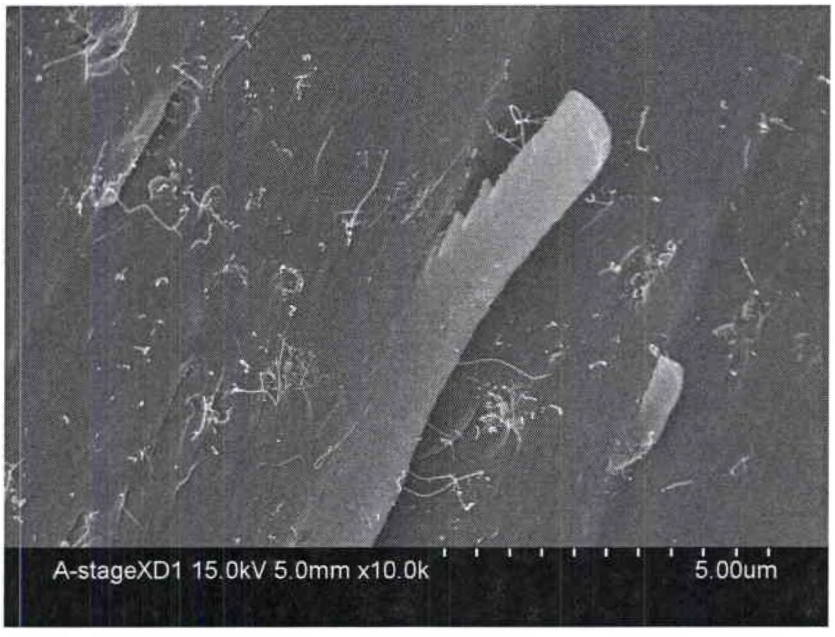

Fig. B.4: 0% Chem-stage fracture surface at 10,000X magnification.

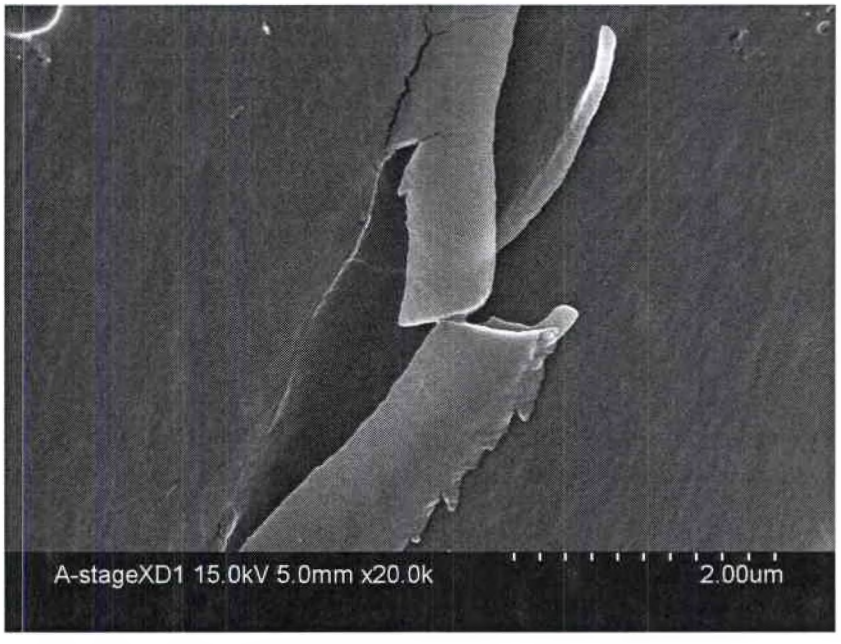

Fig. B.5: 0% Chem-stage fracture surface at 20,000X magnification.

APPENDIX C

5% CHEM-STAGE FRACTURE SURFACES – SEM

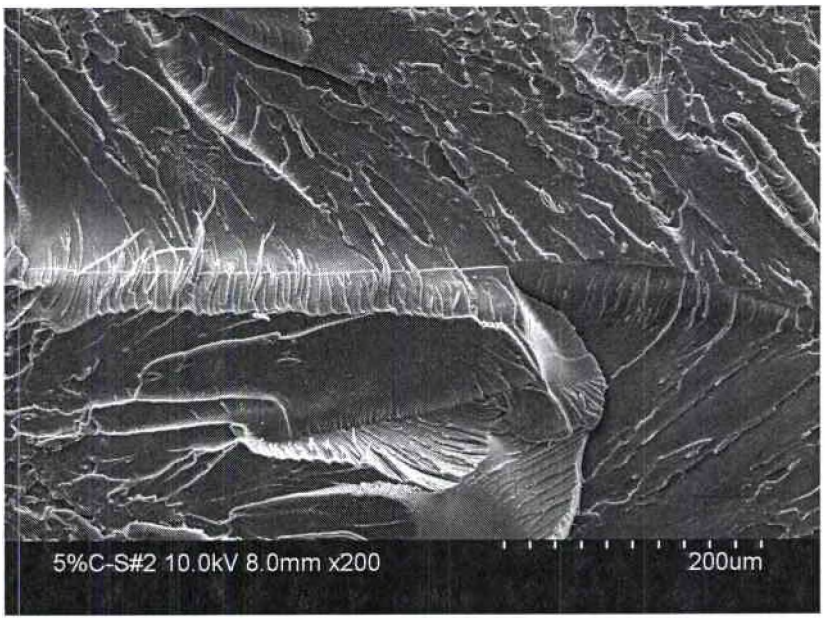

Fig. C.1: 5% Chem-stage fracture surface at 200X magnification.

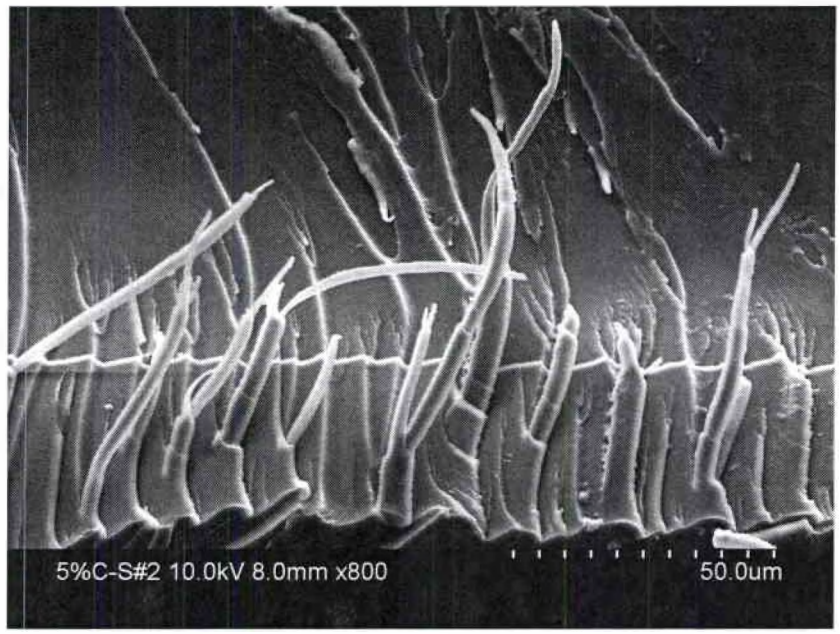

Fig. C.2: 5% Chem-stage fracture surface at 800X magnification.

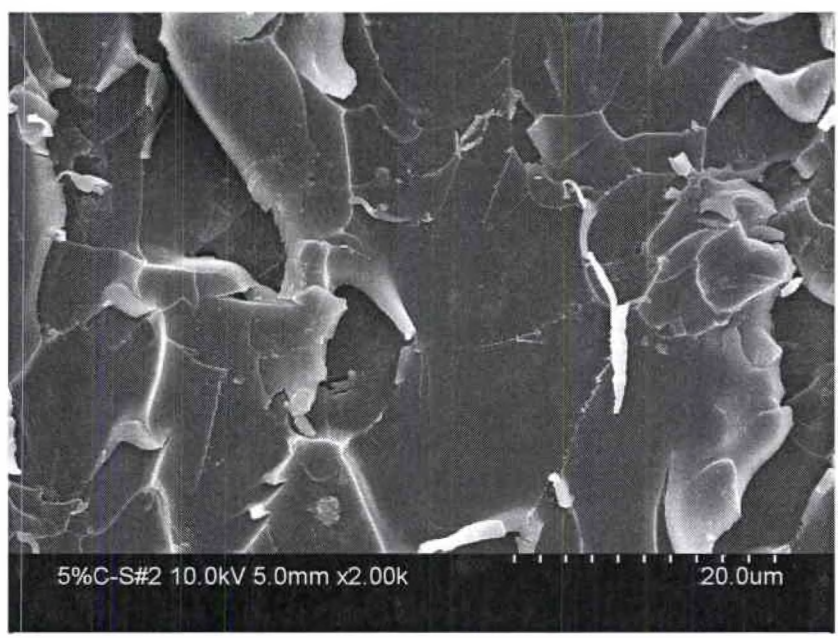

Fig. C.3: 5% Chem-stage fracture surface at 2000X magnification.

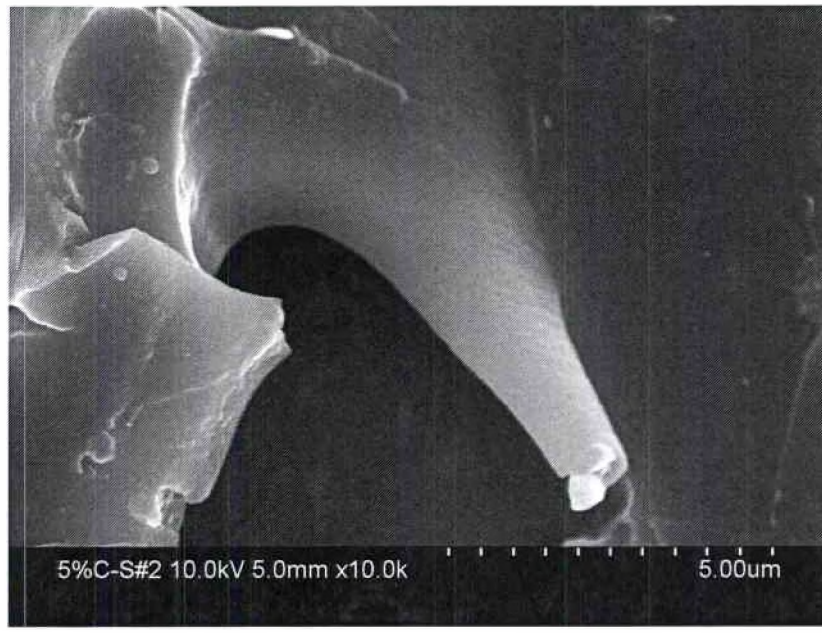

Fig. C.4: 5% Chem-stage fracture surface at 10,000X magnification.

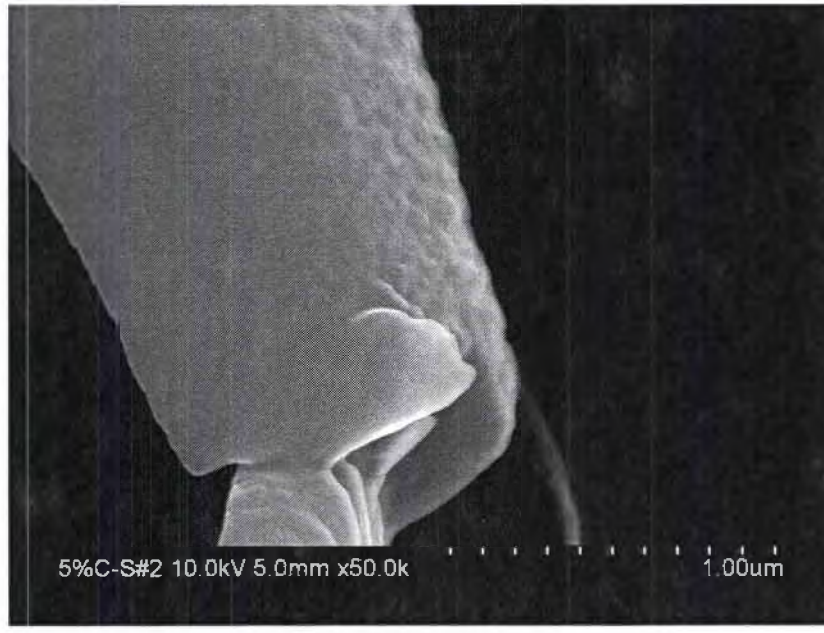

Fig. C.5: 5% Chem-stage fracture surface at 50,000X magnification.

APPENDIX D

15% CHEM-STAGE FRACTURE SURFACES – SEM

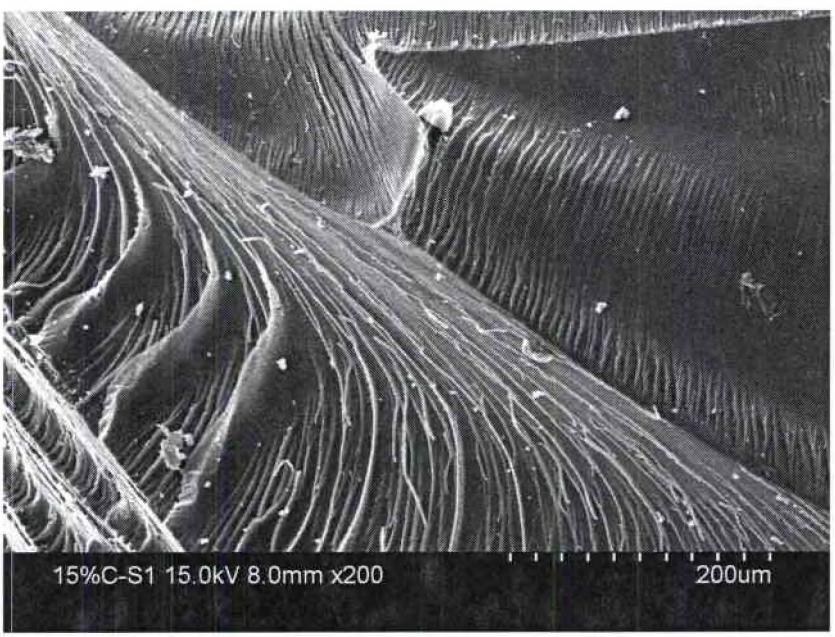

Fig. D.1: 15% Chem-stage fracture surface at 200X magnification.

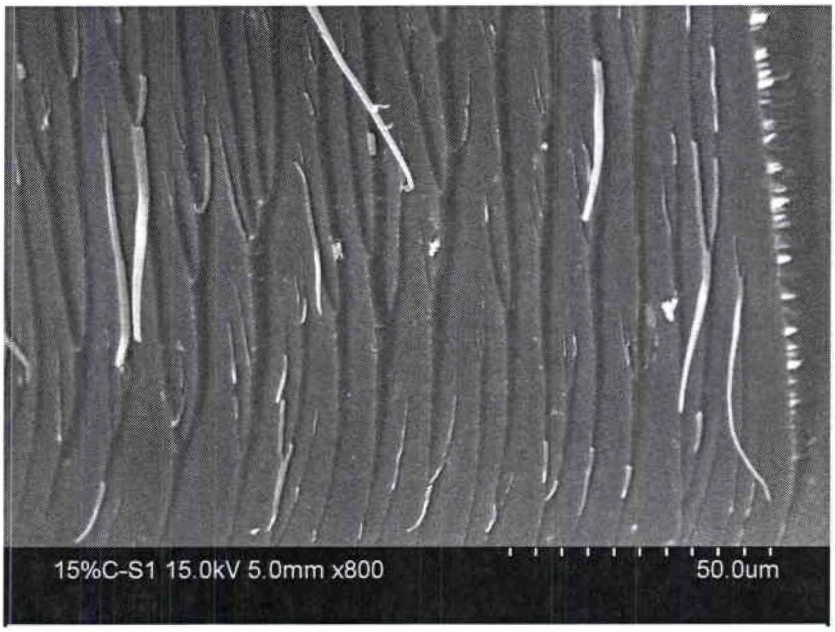

Fig. D.2: 15% Chem-stage fracture surface at 800X magnification.

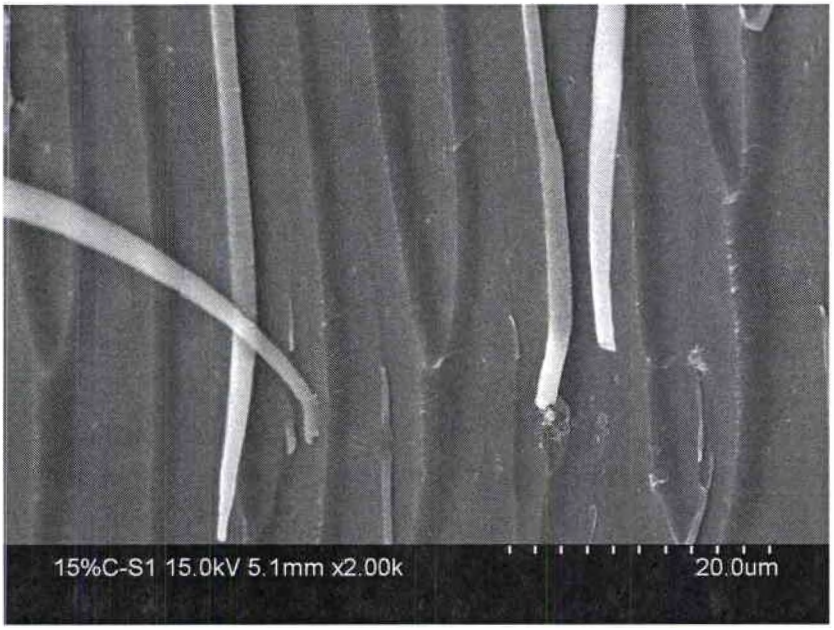

Fig. D.3: 15% Chem-stage fracture surface at 2000X magnification.

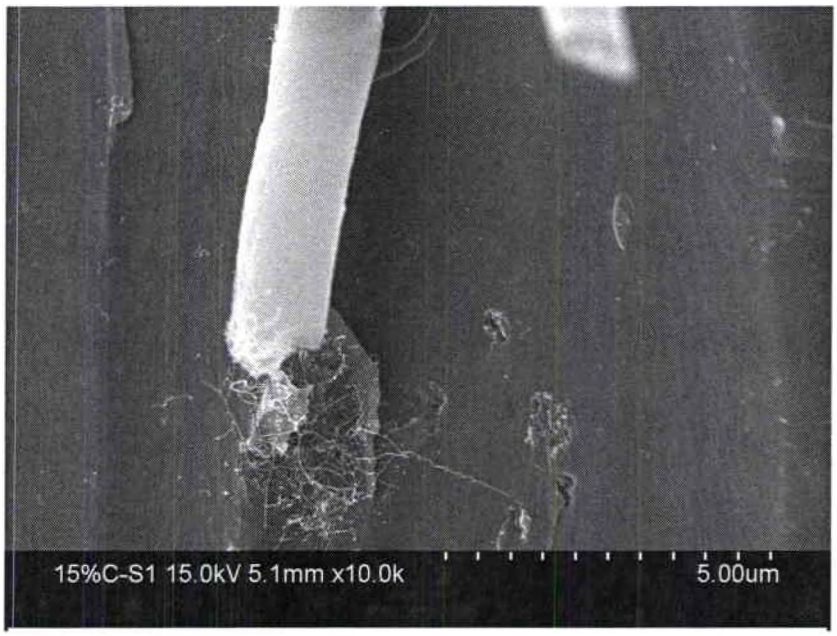

Fig. D.4: 15% Chem-stage fracture surface at 10,000X magnification.

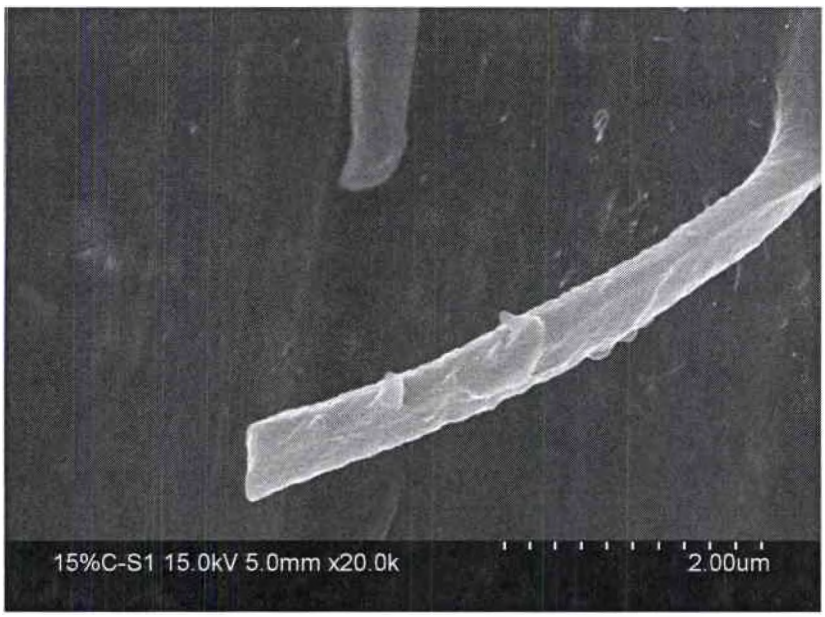

Fig. D.5: 15% Chem-stage fracture surface at 20,000X magnification.

REFERENCES

1. Gojny, F., Nastalczyk, J., Roslaniec, Z., Schulte, K., "Surface Modified Multi-walled Carbon Nanotubes in CNT/Epoxy-composites," *Chemical Physics Letters*, **370**, 820-824 (2003).
2. Thostenson, E., Chou, T., "Processing-structure-multi-functional Property Relationship in Carbon Nanotube/Epoxy Composties," *Carbon*, **44**, 3022-3029 (2006).
3. Thonstenson, E., Ren, Z., Chou, T., "Advances in the Science and Technology of Carbon Nanotubes and their Composites: a review," *Composites Science and Technology*, **61**, 1899-1912 (2001).
4. Thostenson, E., Chou, T., "Nanotube Buckling in Aligned Multi-wall Carbon Nanotube Composties," *Carbon*, **42**, 3015-3018 (2004).
5. Gong, Q., Li, Z., Li, D., Bai, X., Liang, J., "Fabrication and Structure: a study of aligned carbon nanotube/carbon nanocomposites," *Solid State Communications*, **131**, 399-404 (2004).
6. Tibbetts, G., Lake, M., Strong, K., Rice, B., "A Review of the Fabrication and Properties of Vapor-grown Carbon Nanofiber/Polymer Composties," *Composites Science and Technology*, **67**, 1709-1718 (2007).
7. Cooper, C., Cohen, S., Barber, A., Wagner, H., "Detachment of Nanotubes from a Polymer Matrix," *Applied Physics Letters*, **81**, 3873-3875 (2002).
8. Cho, J., Joshi, M., Sun, C, "Effect of Inclusion Size on Mechanical Properties of Polymeric Composites with Micro and Nano Particles," *Composite Science and Technology*, **66**, 1941-1952 (2006).
9. Baggott, J., *Perfect Symmetry: the accidental discovery of the buckminsterfullerene*, Oxford University Press (1994).
10. Saether, E., Frankland, S. Pipes, R., "Transverse mechanical properties of single-walled carbon nanotube crystals. Part I: determination of elastic moduli," *Composites Science and Technology*, **63**, 1543-1550 (2003).
11. Iijima, S., Ichihashi, T., "Single-shell carbon nanotubes of 1-nm diameter," *Nature*, **363**, 603-605 (1993).
12. Gojny, F., Wichmann, M., Fiedler, B., Schulte, K., "Influence of different carbon nanotubes on the mechanical properties of epoxy matrix composites – A comparative study," *Composites Science and Technology*, **65**, 2300-2313 (2005).
13. Klosterman, D. Donaldson, R., Heitkamp, C., Williams, M., Browning, C., "IZOD Impact Testing of Epoxy Resin and Carbon/Epoxy Laminates Containing Carbon Nanofibers or Carbon Nanotubes," *52nd International SAMPE symposium proceedings*, Society for the Advancement of Material and Process Engineering, Baltimore (2007).

14. Gennett, et al, "Formation of Single Wall Carbon Nanotube Superbundles," *Chemistry of Materials*, **12**, 599-601 (2000).
15. Li, C., Chou, T., "Elastic moduli of multi-walled carbon nanotubes and the effect of van der Waals forces," *Composites Science and Technology*, **63**, 1517-1524 (2003).
16. Fiedler, B., Gojny, F., Wichmann, M., Nolte, M., Schulte, K., "Fundamental aspects of nano-reinforced composites," *Composites Science and Technology*, **66**, 3115-3125 (2006).
17. Shackelford, J., *Introduction to Materials Science for Engineers*, Prentice Hall (2000).
18. Ganguli, S., Aglan, H., Dean, D., "Microstructural Origin of Strength and Toughness of Epoxy Nanocomposites," *Journal of Elastomers and Plastics*, **37**, 19-35 (2005).
19. Lin, Y., Zhou, B., Fernando, K., Liu, P., Allard, L., Sun, Y., "Polymeric Carbon Nanocomposites from Carbon Nanotubes Functionalized with Matrix Polymer," *Macromolecules*, **36**, 7199-7204 (2003).
20. Wetzel, B., Rosso, P., Haupert, F., Friedrich, K., "Epoxy nanocomposites – fracture and toughening mechanisms," *Engineering Fracture Mechanics*, **73**, 2375-2398 (2006).
21. Namilae, S., Chandra, N., "Role of atomic scale interfaces in the compressive behavior of carbon nanotubes in composites," *Composites Science and Technology*, **66**, 2030-2038 (2006).
22. Falvo, M., Clary, G., Taylor, R., Chi, V., Brooks, F., Washburn, S., Superfine, R., "Bending and buckling of carbon nanotubes under large strain," *Nature*, **389**, 582-584 (1997).
23. Li, W., Yao, Y., "Laser bending of tubes: mechanism, analysis, and prediction," *Journal of Manufacturing Science and Engineering*, **123**, 674-681 (2001).
24. Maruyama, B., K. Alam, "Carbon Nanotubes and Nanofibers in Composite Materials," *SAMPE Journal*, **38**, No. 3, 59-70 (May/June, 2002).
25. Harris, P.J.F., *Carbon Nanotubes and Related Structures New Materials for the Twenty-First Century*, Cambridge University Press (1999).
26. Lafdi, K., Matzek, M., "Carbon Nanofibers as a Nano-reinforcement for Polymeric Nanocomposites," *35th International SAMPE Technical Conference Proceedings*, Society for the Advancement of Material and Process Engineering, Dayton (2003).
27. Zunjarrao, S., Singh, R., "Characterization of the fracture behavior of epoxy reinforced with nanometer and micrometer sized aluminum particles," *Composites Science and Technology*, **66**, 2296-2305 (2006).